13

Basic Magnetics Theory

Magnetics are an integral part of every switching converter. Often, the design of the magnetic devices cannot be isolated from the converter design. The power electronics engineer must not only model and design the converter, but must model and design the magnetics as well. Modeling and design of magnetics for switching converters is the topic of Part III of this book.

In this chapter, basic magnetics theory is reviewed, including magnetic circuits, inductor modeling, and transformer modeling [1-5]. Loss mechanisms in magnetic devices are described. Winding eddy currents and the proximity effect, a significant loss mechanism in high-current high-frequency windings, are explained in detail [6-11]. Inductor design is introduced in Chapter 14, and transformer design is covered in Chapter 15.

13.1 REVIEW OF BASIC MAGNETICS

13.1.1 Basic Relationships

The basic magnetic quantities are illustrated in Fig. 13.1. Also illustrated are the analogous, and perhaps more familiar, electrical quantities. The *magnetomotive force* $\mathcal{F}$, or scalar potential, between two points x_1 and x_2 is given by the integral of the magnetic field $\boldsymbol{H}$ along a path connecting the points:

$$\mathcal{F} = \int_{x_1}^{x_2} \boldsymbol{H} \cdot d\boldsymbol{\ell} \tag{13.1}$$

where $d\boldsymbol{\ell}$ is a vector length element pointing in the direction of the path. The dot product yields the com-

R. W. Erickson et al., *Fundamentals of Power Electronics*
© Springer Science+Business Media New York 2001

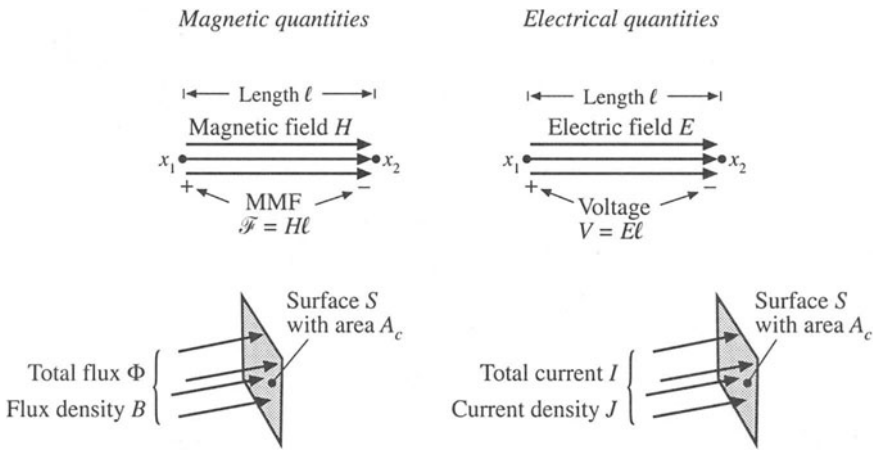

Fig. 13.1 Comparison of magnetic field H, MMF Φ, flux $\mathscr{F}$, and flux density B, with the analogous electrical quantities E, V, I, and J.

ponent of $\boldsymbol{H}$ in the direction of the path. If the magnetic field is of uniform strength H passing through an element of length ℓ as illustrated, then Eq. (13.1) reduces to

$$\mathscr{F} = H\ell \tag{13.2}$$

This is analogous to the electric field of uniform strength E, which induces a voltage $V = E\ell$ between two points separated by distance ℓ.

Figure 13.1 also illustrates a total magnetic flux Φ passing through a surface S having area A_c. The total flux Φ is equal to the integral of the normal component of the flux density B over the surface

$$\Phi = \int_{\text{surface } S} \boldsymbol{B} \cdot d\boldsymbol{A} \tag{13.3}$$

where $d\boldsymbol{A}$ is a vector area element having direction normal to the surface. For a uniform flux density of magnitude B as illustrated, the integral reduces to

$$\Phi = BA_c \tag{13.4}$$

Flux density $\boldsymbol{B}$ is analogous to the electrical current density $\boldsymbol{J}$, and flux Φ is analogous to the electric current I. If a uniform current density of magnitude J passes through a surface of area A_c, then the total current is $I = JA_c$.

Faraday's law relates the voltage induced in a winding to the total flux passing through the interior of the winding. Figure 13.2 illustrates flux $\Phi(t)$ passing through the interior of a loop of wire. The loop encloses cross-sectional area A_c. According to Faraday's law, the flux induces a voltage $v(t)$ in the wire, given by

$$v(t) = \frac{d\Phi(t)}{dt} \tag{13.5}$$

where the polarities of $v(t)$ and $\Phi(t)$ are defined according to the right-hand rule, as in Fig. 13.2. For a

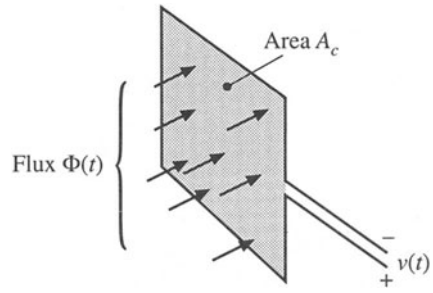

Fig. 13.2 The voltage $v(t)$ induced in a loop of wire is related by Faraday's law to the derivative of the total flux $\Phi(t)$ passing through the interior of the loop.

uniform flux distribution, we can express $v(t)$ in terms of the flux density $B(t)$ by substitution of Eq. (13.4):

$$v(t) = A_c \frac{dB(t)}{dt} \tag{13.6}$$

Thus, the voltage induced in a winding is related to the flux Φ and flux density B passing through the interior of the winding.

Lenz's law states that the voltage $v(t)$ induced by the changing flux $\Phi(t)$ in Fig. 13.2 is of the polarity that tends to drive a current through the loop to counteract the flux change. For example, consider the shorted loop of Fig. 13.3. The changing flux $\Phi(t)$ passing through the interior of the loop induces a voltage $v(t)$ around the loop. This voltage, divided by the impedance of the loop conductor, leads to a current $i(t)$ as illustrated. The current $i(t)$ induces a flux $\Phi'(t)$, which tends to oppose the changes in $\Phi(t)$. Lenz's law is invoked later in this chapter, to provide a qualitative understanding of eddy current phenomena.

Ampere's law relates the current in a winding to the magnetomotive force $\mathcal{F}$ and magnetic field $\boldsymbol{H}$. The net MMF around a closed path of length ℓ_m is equal to the total current passing through the interior of the path. For example, Fig. 13.4 illustrates a magnetic core, in which a wire carrying current $i(t)$ passes through the window in the center of the core. Let us consider the closed path illustrated, which follows the magnetic field lines around the interior of the core. Ampere's law states that

$$\oint_{\text{closed path}} \boldsymbol{H} \cdot d\boldsymbol{\ell} = \text{total current passing through interior of path} \tag{13.7}$$

The total current passing through the interior of the path is equal to the total current passing through the

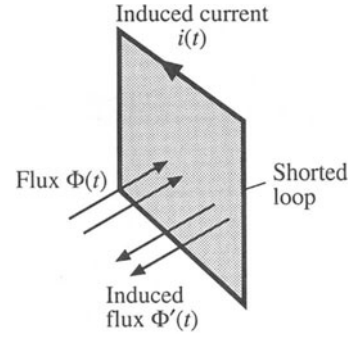

Fig. 13.3 Illustration of Lenz's law in a shorted loop of wire. The flux $\Phi(t)$ induces current $i(t)$, which in turn generates flux $\Phi'(t)$ that tends to oppose changes in $\Phi(t)$.

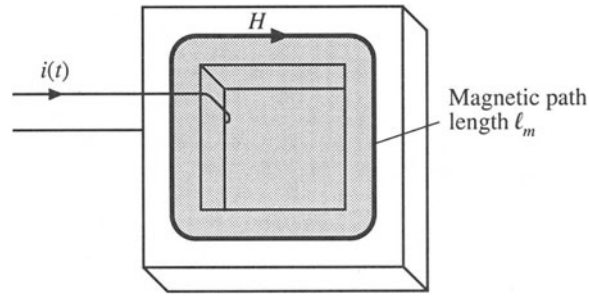

Fig. 13.4 The net MMF around a closed path is related by Ampere's law to the total current passing through the interior of the path.

window in the center of the core, or $i(t)$. If the magnetic field is uniform and of magnitude $H(t)$, then the integral is $H(t)\ell_m$. So for the example of Fig. 13.4, Eq. (13.7) reduces to

$$\mathcal{F}(t) = H(t)\ell_m = i(t) \tag{13.8}$$

Thus, the magnetic field strength $H(t)$ is related to the winding current $i(t)$. We can view winding currents as sources of MMF. Equation (13.8) states that the MMF around the core, $\mathcal{F}(t) = H(t)\ell_m$, is equal to the winding current MMF $i(t)$. The total MMF around the closed loop, accounting for both MMFs, is zero.

The relationship between $\boldsymbol{B}$ and $\boldsymbol{H}$, or equivalently between Φ and $\mathcal{F}$, is determined by the core material characteristics. Figure 13.5(a) illustrates the characteristics of free space, or air:

$$\boldsymbol{B} = \mu_0 \boldsymbol{H} \tag{13.9}$$

The quantity μ_0 is the permeability of free space, and is equal to $4\pi \cdot 10^{-7}$ Henries per meter in MKS units. Figure 13.5(b) illustrates the *B–H* characteristic of a typical iron alloy under high-level sinusoidal steady-state excitation. The characteristic is highly nonlinear, and exhibits both *hysteresis* and *saturation*. The exact shape of the characteristic is dependent on the excitation, and is difficult to predict for arbitrary waveforms.

For purposes of analysis, the core material characteristic of Fig. 13.5(b) is usually modeled by the linear or piecewise-linear characteristics of Fig. 13.6. In Fig. 13.6(a), hysteresis and saturation are ignored. The *B–H* characteristic is then given by

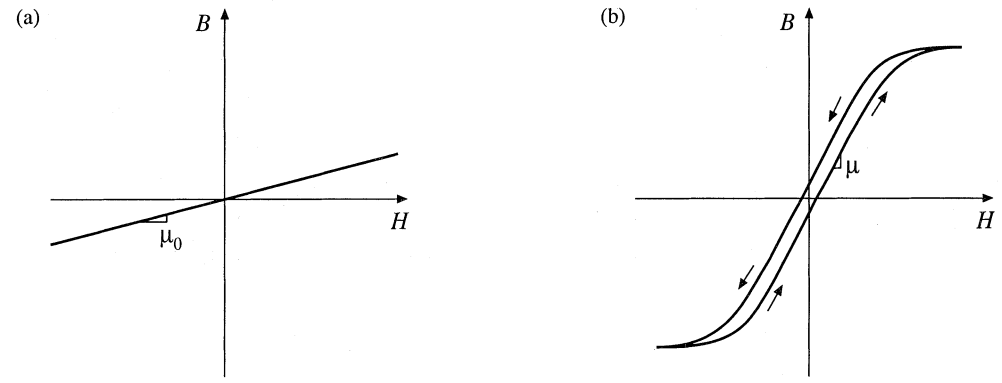

Fig. 13.5 *B–H* characteristics: (a) of free space or air, (b) of a typical magnetic core material.

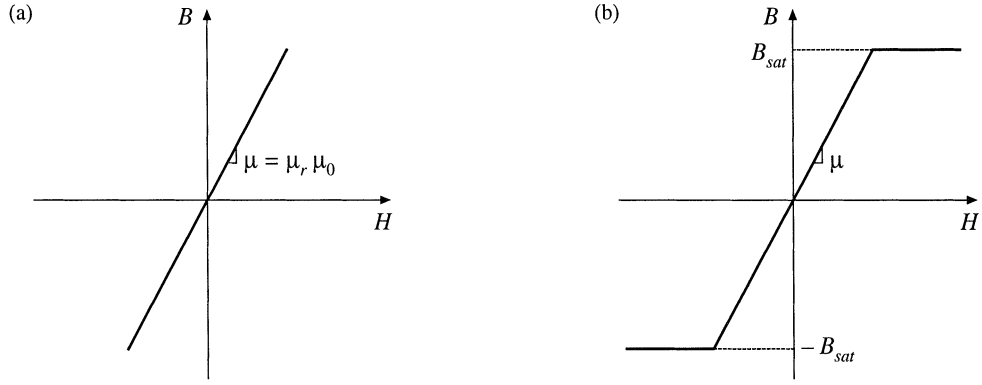

Fig. 13.6 Approximation of the *B–H* characteristics of a magnetic core material: (a) by neglecting both hysteresis and saturation, (b) by neglecting hysteresis.

$$\begin{aligned} \boldsymbol{B} &= \mu \boldsymbol{H} \\ \mu &= \mu_r \mu_0 \end{aligned} \tag{13.10}$$

The core material permeability μ can be expressed as the product of the relative permeability μ_r and of μ_0. Typical values of μ_r lie in the range 10^3 to 10^5.

The piecewise-linear model of Fig. 13.6(b) accounts for saturation but not hysteresis. The core material saturates when the magnitude of the flux density B exceeds the saturation flux density B_{sat}. For $|B| < B_{sat}$, the characteristic follows Eq. (13.10). When $|B| > B_{sat}$, the model predicts that the core reverts to free space, with a characteristic having a much smaller slope approximately equal to μ_0. Square-loop materials exhibit this type of abrupt-saturation characteristic, and additionally have a very large relative permeability μ_r. Soft materials exhibit a less abrupt saturation characteristic, in which μ gradually decreases as H is increased. Typical values of B_{sat} are 1 to 2 Tesla for iron laminations and silicon steel, 0.5 to 1 Tesla for powdered iron and molypermalloy materials, and 0.25 to 0.5 Tesla for ferrite materials.

Unit systems for magnetic quantities are summarized in Table 13.1. The MKS system is used throughout this book. The unrationalized cgs system also continues to find some use. Conversions between these systems are listed.

Figure 13.7 summarizes the relationships between the basic electrical and magnetic quantities of a magnetic device. The winding voltage $v(t)$ is related to the core flux and flux density via Faraday's

Table 13.1 Units for magnetic quantities

Quantity	MKS	Unrationalized cgs	Conversions
Core material equation	$B = \mu_0 \mu_r H$	$B = \mu_r H$	
B	Tesla	Gauss	$1\ \text{T} = 10^4\ \text{G}$
H	Ampere/meter	Oersted	$1\ \text{A/m} = 4\pi \cdot 10^{-3}\ \text{Oe}$
Φ	Weber	Maxwell	$1\ \text{Wb} = 10^8\ \text{Mx}$ $1\ \text{T} = 1\ \text{Wb/m}^2$

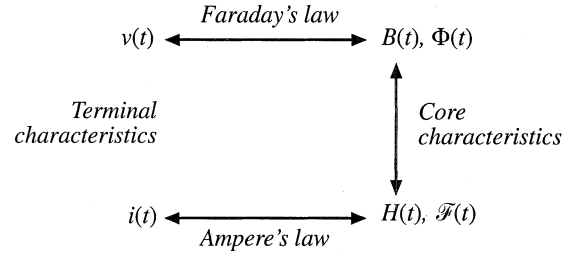

Fig. 13.7 Summary of the steps in determination of the terminal electrical *i–v* characteristics of a magnetic element.

law. The winding current $i(t)$ is related to the magnetic field strength via Ampere's law. The core material characteristics relate B and H.

We can now determine the electrical terminal characteristics of the simple inductor of Fig. 13.8(a). A winding of n turns is placed on a core having permeability μ. Faraday's law states that the flux $\Phi(t)$ inside the core induces a voltage $v_{turn}(t)$ in each turn of the winding, given by

$$v_{turn}(t) = \frac{d\Phi(t)}{dt} \tag{13.11}$$

Since the same flux $\Phi(t)$ passes through each turn of the winding, the total winding voltage is

$$v(t) = nv_{turn}(t) = n\frac{d\Phi(t)}{dt} \tag{13.12}$$

Equation (13.12) can be expressed in terms of the average flux density $B(t)$ by substitution of Eq. (13.4):

$$v(t) = nA_c\frac{dB(t)}{dt} \tag{13.13}$$

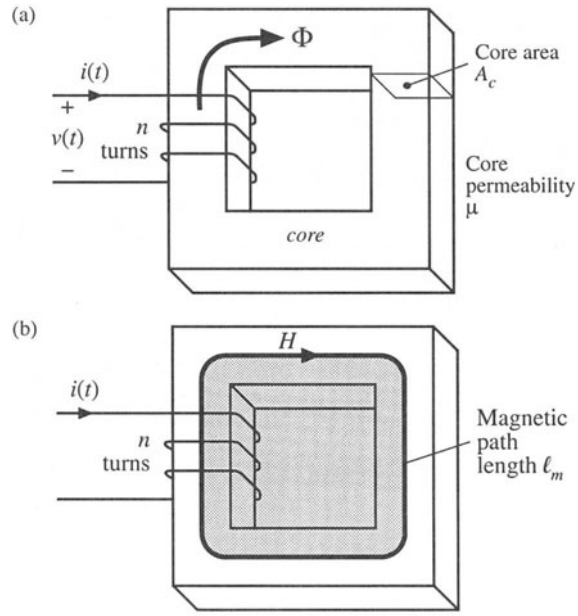

Fig. 13.8 Inductor example: (a) inductor geometry, (b) application of Ampere's law.

where the average flux density $B(t)$ is $\Phi(t)/A_c$.

The use of Ampere's law is illustrated in Fig. 13.8(b). A closed path is chosen which follows an average magnetic field line around the interior of the core. The length of this path is called the *mean magnetic path length* ℓ_m. If the magnetic field strength $H(t)$ is uniform, then Ampere's law states that $H\ell_m$ is equal to the total current passing through the interior of the path, that is, the net current passing through the window in the center of the core. Since there are n turns of wire passing through the window, each carrying current $i(t)$, the net current passing through the window is $ni(t)$. Hence, Ampere's law states that

$$H(t)\ell_m = ni(t) \tag{13.14}$$

Let us model the core material characteristics by neglecting hysteresis but accounting for saturation, as follows:

$$B = \begin{cases} B_{sat} & \text{for } H \geq B_{sat}/\mu \\ \mu H & \text{for } |H| < B_{sat}/\mu \\ -B_{sat} & \text{for } H \leq -B_{sat}/\mu \end{cases} \tag{13.15}$$

The B–H characteristic saturated slope μ_0 is much smaller than μ, and is ignored here. A characteristic similar to Fig. 13.6(b) is obtained. The current magnitude I_{sat} at the onset of saturation can be found by substitution of $H = B_{sat}/\mu$ into Eq. (13.14). The result is

$$I_{sat} = \frac{B_{sat}\ell_m}{\mu n} \tag{13.16}$$

We can now eliminate B and H from Eqs. (13.13) to (13.15), and solve for the electrical terminal characteristics. For $|I| < I_{sat}$, $B = \mu H$. Equation (13.13) then becomes

$$v(t) = \mu n A_c \frac{dH(t)}{dt} \tag{13.17}$$

Substitution of Eq. (13.14) into Eq. (13.17) to eliminate $H(t)$ then leads to

$$v(t) = \frac{\mu n^2 A_c}{\ell_m} \frac{di(t)}{dt} \tag{13.18}$$

which is of the form

$$v(t) = L \frac{di(t)}{dt} \tag{13.19}$$

with

$$L = \frac{\mu n^2 A_c}{\ell_m} \tag{13.20}$$

So the device behaves as an inductor for $|I| < I_{sat}$. When $|I| > I_{sat}$, then the flux density $B(t) = B_{sat}$ is constant. Faraday's law states that the terminal voltage is then

$$v(t) = nA_c \frac{dB_{sat}}{dt} = 0 \tag{13.21}$$

When the core saturates, the magnetic device behavior approaches a short circuit. The device behaves as an inductor only when the winding current magnitude is less than I_{sat}. Practical inductors exhibit some small residual inductance due to their nonzero saturated permeabilities; nonetheless, in saturation the inductor impedance is greatly reduced, and large inductor currents may result.

13.1.2 Magnetic Circuits

Figure 13.9(a) illustrates uniform flux and magnetic field inside a element having permeability μ, length ℓ, and cross-sectional area A_c. The MMF between the two ends of the element is

$$\mathcal{F} = H\ell \tag{13.22}$$

Since $H = B/\mu$ and $B = \Phi/A_c$, we can express $\mathcal{F}$ as

$$\mathcal{F} = \frac{\ell}{\mu A_c}\Phi \tag{13.23}$$

This equation is of the form

$$\mathcal{F} = \Phi\mathcal{R} \tag{13.24}$$

with

$$\mathcal{R} = \frac{\ell}{\mu A_c} \tag{13.25}$$

Equation (13.24) resembles Ohm's law. This equation states that the magnetic flux through an element is proportional to the MMF across the element. The constant of proportionality, or the reluctance $\mathcal{R}$, is analogous to the resistance R of an electrical conductor. Indeed, we can construct a lumped-element magnetic circuit model that corresponds to Eq. (13.24), as in Fig. 13.9(b). In this magnetic circuit model, voltage and current are replaced by MMF and flux, while the element characteristic, Eq. (13.24), is represented by the analog of a resistor, having reluctance $\mathcal{R}$.

Complicated magnetic structures, composed of multiple windings and multiple heterogeneous

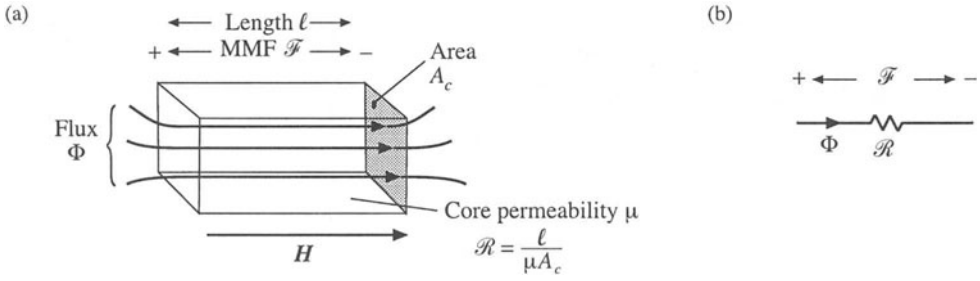

Fig. 13.9 An element containing magnetic flux (a), and its equivalent magnetic circuit (b).

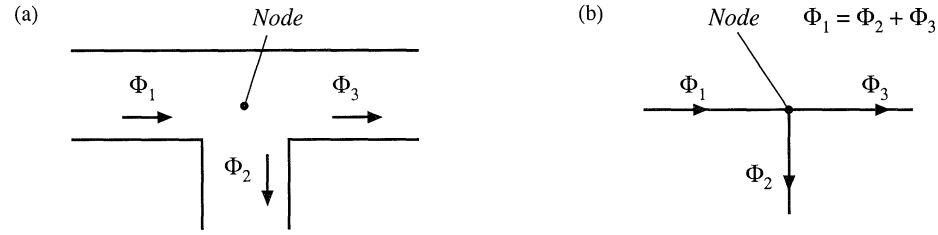

Fig. 13.10 Kirchoff's current law, applied to magnetic circuits: the net flux entering a node must be zero: (a) physical element, in which three legs of a core meet at a node; (b) magnetic circuit model.

elements such as cores and air gaps, can be represented using equivalent magnetic circuits. These magnetic circuits can then be solved using conventional circuit analysis, to determine the various fluxes, MMFs, and terminal voltages and currents. Kirchoff's laws apply to magnetic circuits, and follow directly from Maxwell's equations. The analog of Kirchoff's current law holds because the divergence of $\boldsymbol{B}$ is zero, and hence magnetic flux lines are continuous and cannot end. Therefore, any flux line that enters a node must leave the node. As illustrated in Fig. 13.10, the total flux entering a node must be zero. The analog of Kirchoff's voltage law follows from Ampere's law, Eq. (13.7). The left-hand-side integral in Eq. (13.7) is the sum of the MMFs across the reluctances around the closed path. The right-hand-side of Eq. (13.7) states that currents in windings are sources of MMF. An n-turn winding carrying current $i(t)$ can be modeled as an MMF source, analogous to a voltage source, of value $ni(t)$. When these MMF sources are included, the total MMF around a closed path is zero.

Consider the inductor with air gap of Fig. 13.11(a). A closed path following the magnetic field lines is illustrated. This path passes through the core, of permeability μ and length ℓ_c, and across the air gap, of permeability μ_0 and length ℓ_g. The cross-sectional areas of the core and air gap are approximately equal. Application of Ampere's law for this path leads to

$$\mathcal{F}_c + \mathcal{F}_g = ni \tag{13.26}$$

where $\mathcal{F}_c$ and $\mathcal{F}_g$ are the MMFs across the core and air gap, respectively. The core and air gap characteristics can be modeled by reluctances as in Fig. 13.9 and Eq. (13.25); the core reluctance $\mathcal{R}_c$ and air gap reluctance $\mathcal{R}_g$ are given by

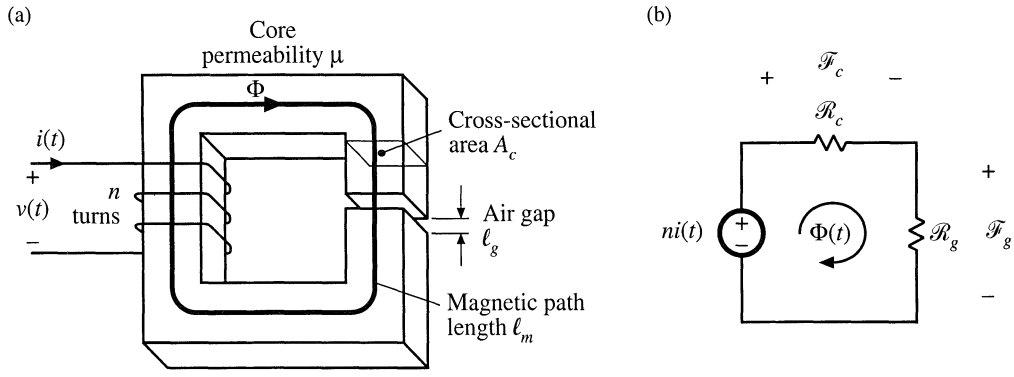

Fig. 13.11 Inductor with air gap example: (a) physical geometry, (b) magnetic circuit model.

$$\mathcal{R}_c = \frac{\ell_c}{\mu A_c}$$
$$\mathcal{R}_g = \frac{\ell_g}{\mu_0 A_c} \tag{13.27}$$

A magnetic circuit corresponding to Eqs. (13.26) and (13.27) is given in Fig. 13.11(b). The winding is a source of MMF, of value ni. The core and air gap reluctances are effectively in series. The solution of the magnetic circuit is

$$ni = \Phi\left(\mathcal{R}_c + \mathcal{R}_g\right) \tag{13.28}$$

The flux $\Phi(t)$ passes through the winding, and so we can use Faraday's law to write

$$v(t) = n\frac{d\Phi(t)}{dt} \tag{13.29}$$

Use of Eq. (13.28) to eliminate $\Phi(t)$ yields

$$v(t) = \frac{n^2}{\mathcal{R}_c + \mathcal{R}_g}\frac{di(t)}{dt} \tag{13.30}$$

Therefore, the inductance L is

$$L = \frac{n^2}{\mathcal{R}_c + \mathcal{R}_g} \tag{13.31}$$

The air gap increases the total reluctance of the magnetic circuit, and decreases the inductance.

Air gaps are employed in practical inductors for two reasons. With no air gap ($\mathcal{R}_g = 0$), the inductance is directly proportional to the core permeability μ. This quantity is dependent on temperature and operating point, and is difficult to control. Hence, it may be difficult to construct an inductor having a well-controlled value of L. Addition of an air gap having a reluctance $\mathcal{R}_g$ greater than $\mathcal{R}_c$ causes the value of L in Eq. (13.31) to be insensitive to variations in μ.

Addition of an air gap also allows the inductor to operate at higher values of winding current $i(t)$ without saturation. The total flux Φ is plotted vs. the winding MMF ni in Fig. 13.12. Since Φ is proportional to B, and when the core is not saturated ni is proportional to the magnetic field strength H in the

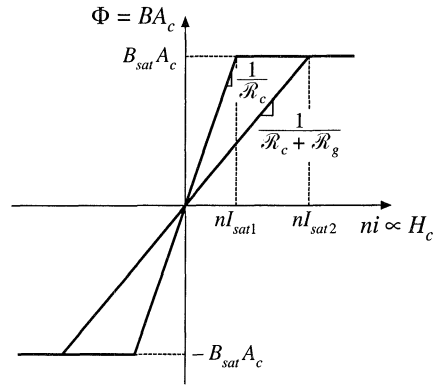

Fig. 13.12 Effect of air gap on the magnetic circuit Φ vs. ni characteristics. The air gap increases the current I_{sat} at the onset of core saturation.

core, Fig. 13.12 has the same shape as the core *B–H* characteristic. When the core is not saturated, Φ is related to *ni* according to the linear relationship of Eq. (13.28). When the core saturates, Φ is equal to

$$\Phi_{sat} = B_{sat} A_c \tag{13.32}$$

The winding current I_{sat} at the onset of saturation is found by substitution of Eq. (13.32) into (13.28):

$$I_{sat} = \frac{B_{sat} A_c}{n} \left(\mathcal{R}_c + \mathcal{R}_g \right) \tag{13.33}$$

The Φ–*ni* characteristics are plotted in Fig. 13.12 for two cases: (a) air gap present, and (b) no air gap ($\mathcal{R}_g = 0$). It can be seen that I_{sat} is increased by addition of an air gap. Thus, the air gap allows increase of the saturation current, at the expense of decreased inductance.

13.2 TRANSFORMER MODELING

Consider next the two-winding transformer of Fig. 13.13. The core has cross-sectional area A_c, mean magnetic path length ℓ_m, and permeability μ. An equivalent magnetic circuit is given in Fig. 13.14. The core reluctance is

$$\mathcal{R} = \frac{\ell_m}{\mu A_c} \tag{13.34}$$

Since there are two windings in this example, it is necessary to determine the relative polarities of the MMF generators. Ampere's law states that

$$\mathcal{F}_c = n_1 i_1 + n_2 i_2 \tag{13.35}$$

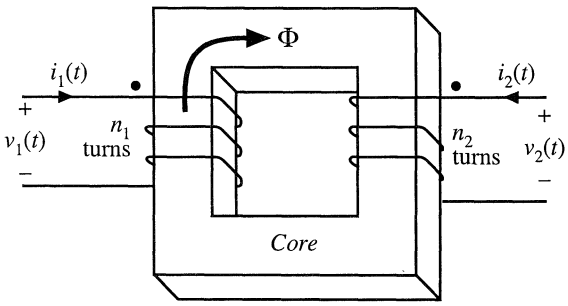

Fig. 13.13 A two-winding transformer.

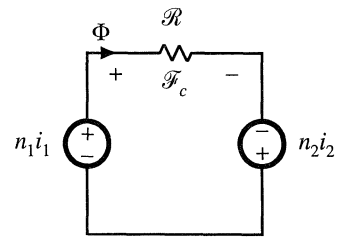

Fig. 13.14 Magnetic circuit that models the two-winding transformer of Fig. 13.13.

The MMF generators are additive, because the currents i_1 and i_2 pass in the same direction through the core window. Solution of Fig. 13.14 yields

$$\Phi\mathcal{R} = n_1 i_1 + n_2 i_2 \tag{13.36}$$

This expression could also be obtained by substitution of $\mathcal{F}_c = \Phi\mathcal{R}$ into Eq. (13.35).

13.2.1 The Ideal Transformer

In the ideal transformer, the core reluctance $\mathcal{R}$ approaches zero. The causes the core MMF $\mathcal{F}_c = \Phi\mathcal{R}$ to also approach zero. Equation (13.35) then becomes

$$0 = n_1 i_1 + n_2 i_2 \tag{13.37}$$

Also, by Faraday's law, we have

$$\begin{aligned} v_1 &= n_1 \frac{d\Phi}{dt} \\ v_2 &= n_2 \frac{d\Phi}{dt} \end{aligned} \tag{13.38}$$

Note that Φ is the same in both equations above: the same total flux links both windings. Elimination of Φ leads to

$$\frac{d\Phi}{dt} = \frac{v_1}{n_1} = \frac{v_2}{n_2} \tag{13.39}$$

Equations (13.37) and (13.39) are the equations of the ideal transformer:

$$\frac{v_1}{n_1} = \frac{v_2}{n_2} \quad \text{and} \quad n_1 i_1 + n_2 i_2 = 0 \tag{13.40}$$

The ideal transformer symbol of Fig. 13.15 is defined by Eq. (13.40).

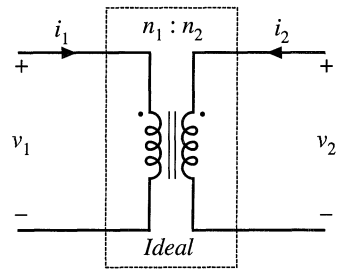

Fig. 13.15 Ideal transformer symbol.

13.2.2 The Magnetizing Inductance

For the actual case in which the core reluctance $\mathcal{R}$ is nonzero, we have

$$\Phi\mathcal{R} = n_1 i_1 + n_2 i_2 \quad \text{with} \quad v_1 = n_1 \frac{d\Phi}{dt} \tag{13.41}$$

Elimination of Φ yields

$$v_1 = \frac{n_1^2}{\mathcal{R}} \frac{d}{dt}\left[i_1 + \frac{n_2}{n_1} i_2 \right] \tag{13.42}$$

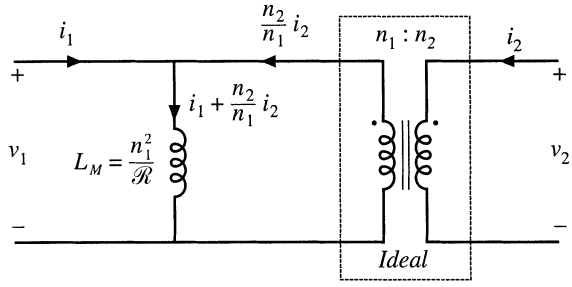

Fig. 13.16 Transformer model including magnetizing inductance.

This equation is of the form

$$v_1 = L_M \frac{di_M}{dt} \tag{13.43}$$

where

$$\begin{aligned} L_M &= \frac{n_1^2}{\mathcal{R}} \\ i_M &= i_1 + \frac{n_2}{n_1} i_2 \end{aligned} \tag{13.44}$$

are the *magnetizing inductance* and *magnetizing current*, referred to the primary winding. An equivalent circuit is illustrated in Fig. 13.16.

Figure 13.16 coincides with the transformer model introduced in Chapter 6. The magnetizing inductance models the magnetization of the core material. It is a real, physical inductor, which exhibits saturation and hysteresis. All physical transformers must contain a magnetizing inductance. For example, suppose that we disconnect the secondary winding. We are then left with a single winding on a magnetic core—an inductor. Indeed, the equivalent circuit of Fig. 13.16 predicts this behavior, via the magnetizing inductance. The magnetizing current causes the ratio of the winding currents to differ from the turns ratio.

The transformer saturates when the core flux density $B(t)$ exceeds the saturation flux density B_{sat}. When the transformer saturates, the magnetizing current $i_M(t)$ becomes large, the impedance of the magnetizing inductance becomes small, and the transformer windings become short circuits. It should be noted that large winding currents $i_1(t)$ and $i_2(t)$ do not necessarily cause saturation: if these currents obey Eq. (13.37), then the magnetizing current is zero and there is no net magnetization of the core. Rather, saturation of a transformer is a function of the applied volt-seconds. The magnetizing current is given by

$$i_M(t) = \frac{1}{L_M} \int v_1(t) dt \tag{13.45}$$

Alternatively, Eq. (13.45) can be expressed in terms of the core flux density $B(t)$ as

$$B(t) = \frac{1}{n_1 A_c} \int v_1(t) dt \tag{13.46}$$

The flux density and magnetizing current will become large enough to saturate the core when the applied volt-seconds λ_1 is too large, where λ_1 is defined for a periodic ac voltage waveform as

$$\lambda_1 = \int_{t_1}^{t_2} v_1(t)dt \tag{13.47}$$

The limits are chosen such that the integral is taken over the positive portion of the applied periodic voltage waveform.

To fix a saturating transformer, the flux density should be decreased by increasing the number of turns, or by increasing the core cross-sectional area A_c. Adding an air gap has no effect on saturation of conventional transformers, since it does not modify Eq. (13.46). An air gap simply makes the transformer less ideal, by decreasing L_M and increasing $i_M(t)$ without changing $B(t)$. Saturation mechanisms in transformers differ from those of inductors, because transformer saturation is determined by the applied winding voltage waveforms, rather than the applied winding currents.

13.2.3 Leakage Inductances

In practice, there is some flux which links one winding but not the other, by "leaking" into the air or by some other mechanism. As illustrated in Fig. 13.17, this flux leads to *leakage inductance*, i.e., additional effective inductances that are in series with the windings. A topologically equivalent structure is illustrated in Fig. 13.17(b), in which the leakage fluxes $\Phi_{\ell 1}$ and $\Phi_{\ell 2}$ are shown explicitly as separate inductors.

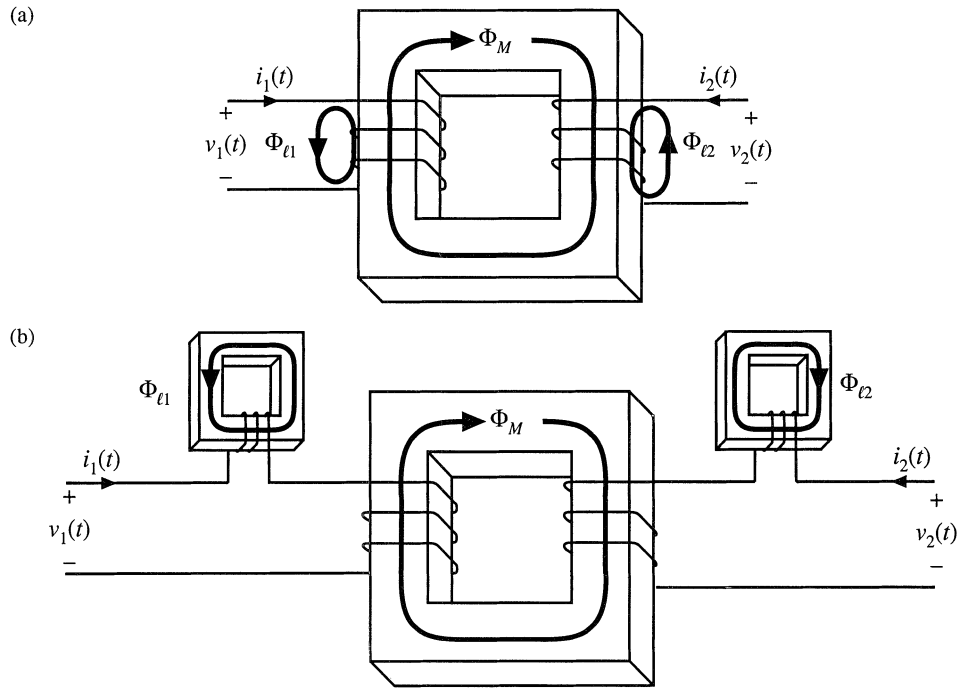

Fig. 13.17 Leakage flux in a two-winding transformer: (a) transformer geometry, (b) an equivalent system.

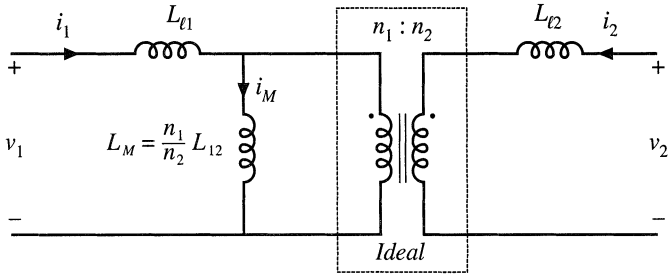

Fig. 13.18 Two-winding transformer equivalent circuit, including magnetizing inductance referred to primary, and primary and secondary leakage inductances.

Figure 13.18 illustrates a transformer electrical equivalent circuit model, including series inductors $L_{\ell 1}$ and $L_{\ell 2}$ which model the leakage inductances. These leakage inductances cause the terminal voltage ratio $v_2(t)/v_1(t)$ to differ from the ideal turns ratio n_2/n_1. In general, the terminal equations of a two-winding transformer can be written

$$\begin{bmatrix} v_1(t) \\ v_2(t) \end{bmatrix} = \begin{bmatrix} L_{11} & L_{12} \\ L_{12} & L_{22} \end{bmatrix} \frac{d}{dt} \begin{bmatrix} i_1(t) \\ i_2(t) \end{bmatrix} \tag{13.48}$$

The quantity L_{12} is called the *mutual inductance*, and is given by

$$L_{12} = \frac{n_1 n_2}{\mathcal{R}} = \frac{n_2}{n_1} L_M \tag{13.49}$$

The quantities L_{11} and L_{22} are called the primary and secondary *self-inductances*, given by

$$\begin{aligned} L_{11} &= L_{\ell 1} + \frac{n_1}{n_2} L_{12} \\ L_{22} &= L_{\ell 2} + \frac{n_2}{n_1} L_{12} \end{aligned} \tag{13.50}$$

Note that Eq. (13.48) does not explicitly identify the physical turns ratio n_2/n_1. Rather, Eq. (13.48) expresses the transformer behavior as a function of electrical quantities alone. Equation (13.48) can be used, however, to define the *effective turns ratio*

$$n_e = \sqrt{\frac{L_{22}}{L_{11}}} \tag{13.51}$$

and the *coupling coefficient*

$$k = \frac{L_{12}}{\sqrt{L_{11} L_{22}}} \tag{13.52}$$

The coupling coefficient k lies in the range $0 \leq k \leq 1$, and is a measure of the degree of magnetic coupling between the primary and secondary windings. In a transformer with perfect coupling, the leakage inductances $L_{\ell 1}$ and $L_{\ell 2}$ are zero. The coupling coefficient k is then equal to 1. Construction of low-voltage transformers having coupling coefficients in excess of 0.99 is quite feasible. When the coupling coefficient is close to 1, then the effective turns ratio n_e is approximately equal to the physical turns ratio n_2/n_1.

13.3 LOSS MECHANISMS IN MAGNETIC DEVICES

13.3.1 Core Loss

Energy is required to effect a change in the magnetization of a core material. Not all of this energy is recoverable in electrical form; a fraction is lost as heat. This power loss can be observed electrically as hysteresis of the *B–H* loop.

Consider an n–turn inductor excited by periodic waveforms $v(t)$ and $i(t)$ having frequency f. The net energy that flows into the inductor over one cycle is

$$W = \int_{\text{one cycle}} v(t)i(t)\,dt \tag{13.53}$$

We can relate this expression to the core *B–H* characteristic: substitute $B(t)$ for $v(t)$ using Faraday's law, Eq. (13.13), and substitute $H(t)$ for $i(t)$ using Ampere's law, i.e. Eq. (13.14):

$$\begin{aligned} W &= \int_{\text{one cycle}} \left(nA_c \frac{dB(t)}{dt}\right)\left(\frac{H(t)\ell_m}{n}\right)dt \\ &= \left(A_c\ell_m\right)\int_{\text{one cycle}} H\,dB \end{aligned} \tag{13.54}$$

The term $A_c\ell_m$ is the volume of the core, while the integral is the area of the *B–H* loop:

$$\text{(energy lost per cycle)} = \text{(core volume)(area of } B\text{–}H \text{ loop)} \tag{13.55}$$

The *hysteresis power loss* P_H is equal to the energy lost per cycle, multiplied by the excitation frequency f:

$$P_H = (f)\left(A_c\ell_m\right)\int_{\text{one cycle}} H\,dB \tag{13.56}$$

To the extent that the size of the hysteresis loop is independent of frequency, hysteresis loss increases directly with operating frequency.

Magnetic core materials are iron alloys that, unfortunately, are also good electrical conductors. As a result, ac magnetic fields can cause electrical *eddy currents* to flow within the core material itself. An example is illustrated in Fig. 13.19. The ac flux $\Phi(t)$ passes through the core. This induces eddy currents $i(t)$ which, according to Lenz's law, flow in paths that oppose the time-varying flux $\Phi(t)$. These eddy currents cause i^2R losses in the resistance of the core material. The eddy current losses are especially significant in high-frequency applications.

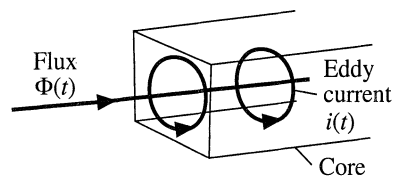

Fig. 13.19 Eddy currents in an iron core.

According to Faraday's law, the ac flux $\Phi(t)$ induces voltage in the core, which drives the current around the paths illustrated in Fig. 13.19. Since the induced voltage is proportional to the derivative of the flux, the voltage magnitude increases directly with the excitation frequency f. If the impedance of

the core material is purely resistive and independent of frequency, then the magnitude of the induced eddy currents also increases directly with f. This implies that the i^2R eddy current losses should increase as f^2. In power ferrite materials, the core material impedance magnitude actually decreases with increasing f. Over the useful frequency range, the eddy current losses typically increase faster than f^2.

There is a basic tradeoff between saturation flux density and core loss. Use of a high operating flux density leads to reduced size, weight, and cost. Silicon steel and similar materials exhibit saturation flux densities of 1.5 to 2 T. Unfortunately, these core materials exhibit high core loss. In particular, the low resistivity of these materials leads to high eddy current loss. Hence, these materials are suitable for filter inductor and low-frequency transformer applications. The core material is produced in laminations or thin ribbons, to reduce the eddy current magnitude. Other ferrous alloys may contain molybdenum, cobalt, or other elements, and exhibit somewhat lower core loss as well as somewhat lower saturation flux densities.

Iron alloys are also employed in powdered cores, containing ferromagnetic particles of sufficiently small diameter such that eddy currents are small. These particles are bound together using an insulating medium. Powdered iron and molybdenum permalloy powder cores exhibit typical saturation flux densities of 0.6 to 0.8 T, with core losses significantly lower than laminated ferrous alloy materials. The insulating medium behaves effectively as a distributed air gap, and hence these cores have relatively low permeability. Powder cores find application as transformers at frequencies of several kHz, and as filter inductors in high frequency (100 kHz) switching converters.

Amorphous alloys exhibit low hysteresis loss. Core conductivity and eddy current losses are somewhat lower than ferrous alloys, but higher than ferrites. Saturation flux densities in the range 0.6 to 1.5 T are obtained.

Ferrite cores are ceramic materials having low saturation flux density, 0.25 to 0.5 T. Their resistivities are much higher than other materials, and hence eddy current losses are much smaller. Manganese-zinc ferrite cores find widespread use as inductors and transformers in converters having switching frequencies of 10 kHz to 1 MHz. Nickel-zinc ferrite materials can be employed at yet higher frequencies.

Figure 13.20 contains typical total core loss data, for a certain ferrite material. Power loss density, in Watts per cubic centimeter of core material, is plotted as a function of sinusoidal excitation frequency f and peak ac flux density ΔB. At a given frequency, the core loss P_{fe} can be approximated by an empirical function of the form

$$P_{fe} = K_{fe}(\Delta B)^{\beta} A_c \ell_m \qquad (13.57)$$

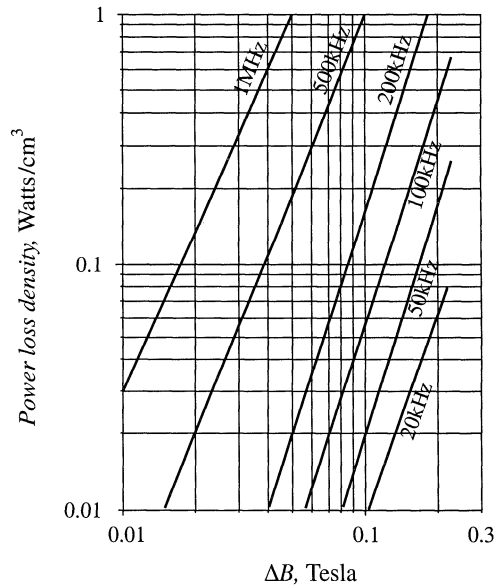

Fig. 13.20 Typical core loss data for a high-frequency power ferrite material. Power loss density is plotted vs. peak ac flux density ΔB, for sinusoidal excitation.

The parameters K_{fe} and β are determined by fitting Eq. (13.57) to the manufacturer's published data. Typical values of β for ferrite materials operating in their intended range of ΔB and f lie in the range 2.6 to 2.8. The constant of proportionality K_{fe} increases rapidly with excitation frequency f. The dependence of K_{fe} on f can also be approximated by empirical formulae that are fitted to the manu-

facturer's published data; a fourth-order polynomial or a function of the form $K_{fe0} f^{\xi}$ are sometimes employed for this purpose.

13.3.2 Low-Frequency Copper Loss

Significant loss also occurs in the resistance of the copper windings. This is also a major determinant of the size of a magnetic device: if copper loss and winding resistance were irrelevant, then inductor and transformer elements could be made arbitrarily small by use of many small turns of small wire.

Figure 13.21 contains an equivalent circuit of a winding, in which element R models the winding resistance. The copper loss of the winding is

$$P_{cu} = I_{rms}^2 R \tag{13.58}$$

where I_{rms} is the rms value of $i(t)$. The dc resistance of the winding conductor can be expressed as

$$R = \rho \frac{\ell_b}{A_w} \tag{13.59}$$

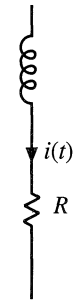

Fig. 13.21 Winding equivalent circuit that models copper loss.

where A_w is the wire bare cross-sectional area, and ℓ_b is the length of the wire. The resistivity ρ is equal to $1.724 \cdot 10^{-6}$ Ω–cm for soft-annealed copper at room temperature. This resistivity increases to $2.3 \cdot 10^{-6}$ Ω–cm at 100°C.

13.4 EDDY CURRENTS IN WINDING CONDUCTORS

Eddy currents also cause power losses in winding conductors. This can lead to copper losses significantly in excess of the value predicted by Eqs. (13.58) and (13.59). The specific conductor eddy current mechanisms are called the *skin effect* and the *proximity effect*. These mechanisms are most pronounced in high-current conductors of multi-layer windings, particularly in high-frequency converters.

13.4.1 Introduction to the Skin and Proximity Effects

Figure 13.22(a) illustrates a current $i(t)$ flowing through a solitary conductor. This current induces magnetic flux $\Phi(t)$, whose flux lines follow circular paths around the current as shown. According to Lenz's law, the ac flux in the conductor induces eddy currents, which flow in a manner that tends to oppose the ac flux $\Phi(t)$. Figure 13.22(b) illustrates the paths of the eddy currents. It can be seen that the eddy currents tend to reduce the net current density in the center of the conductor, and increase the net current density near the surface of the conductor.

The current distribution within the conductor can be found by solution of Maxwell's equations. For a sinusoidal current $i(t)$ of frequency f, the result is that the current density is greatest at the surface of the conductor. The current density is an exponentially decaying function of distance into the conductor, with characteristic length δ known as the *penetration depth* or *skin depth*. The penetration depth is given by

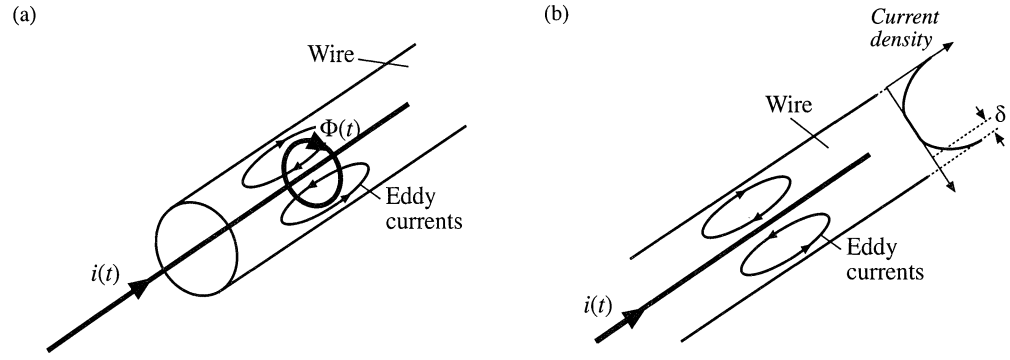

Fig. 13.22 The skin effect: (a) current $i(t)$ induces flux $\Phi(t)$, which in turn induces eddy currents in conductor; (b) the eddy currents tend to oppose the current $i(t)$ in the center of the wire, and increase the current on the surface of the wire.

$$\delta = \sqrt{\frac{\rho}{\pi \mu f}} \tag{13.60}$$

For a copper conductor, the permeability μ is equal to μ_0, and the resistivity ρ is given in Section 13.3.2. At 100°C, the penetration depth of a copper conductor is

$$\delta = \frac{7.5}{\sqrt{f}} \text{ cm} \tag{13.61}$$

with f expressed in Hz. The penetration depth of copper conductors is plotted in Fig. 13.23, as a function of frequency f. For comparison, the wire diameters d of standard American Wire Gauge (AWG) conductors are also listed. It can be seen that $d/\delta = 1$ for AWG #40 at approximately 500 kHz, while $d/\delta = 1$ for

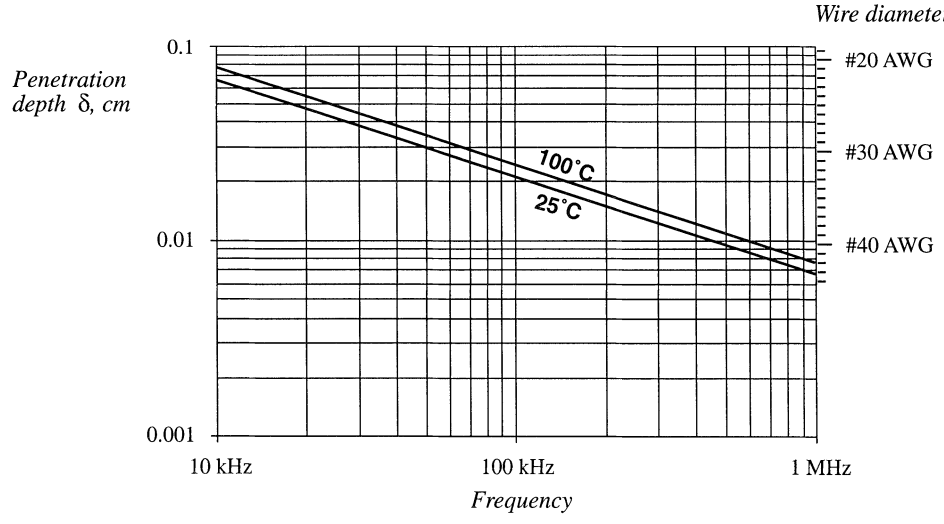

Fig. 13.23 Penetration depth δ, as a function of frequency f, for copper wire.

AWG #22 at approximately 10 kHz.

The skin effect causes the resistance and copper loss of solitary large-diameter wires to increase at high frequency. High-frequency currents do not penetrate to the center of the conductor. The current crowds at the surface of the wire, the inside of the wire is not utilized, and the effective wire cross-sectional area is reduced. However, the skin effect alone is not sufficient to explain the increased high-frequency copper losses observed in multiple-layer transformer windings.

A conductor that carries a high-frequency current $i(t)$ induces copper loss in a adjacent conductor by a phenomenon known as the *proximity effect*. Figure 13.24 illustrates two copper foil conductors that are placed in close proximity to each other. Conductor 1 carries a high-frequency sinusoidal current $i(t)$, whose penetration depth δ is much smaller than the thickness h of conductors 1 or 2. Conductor 2 is open-circuited, so that it carries a net current of zero. However, it is possible for eddy currents to be induced in conductor 2 by the current $i(t)$ flowing in conductor 1.

The current $i(t)$ flowing in conductor 1 generates a flux $\Phi(t)$ in the space between conductors 1 and 2; this flux attempts to penetrate conductor 2. By Lenz's law, a current is induced on the adjacent (left) side of conductor 2, which tends to oppose the flux $\Phi(t)$. If the conductors are closely spaced, and if $h \gg \delta$, then the induced current will be equal and opposite to the current $i(t)$, as illustrated in Fig. 13.24.

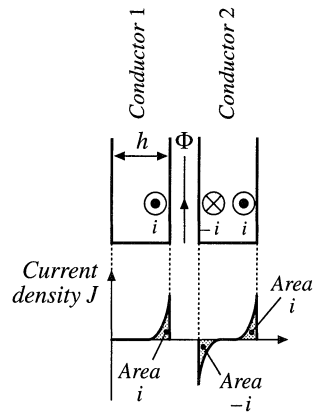

Fig. 13.24 The proximity effect in adjacent copper foil conductors. Conductor 1 carries current $i(t)$. Conductor 2 is open-circuited.

Since conductor 2 is open-circuited, the net current in conductor 2 must be zero. Therefore, a current + $i(t)$ flows on the right-side surface of conductor 2. So the current flowing in conductor 1 induces a current that circulates on the surfaces of conductor 2.

Figure 13.25 illustrates the proximity effect in a simple transformer winding. The primary winding consists of three series-connected turns of copper foil, having thickness $h \gg \delta$, and carrying net current $i(t)$. The secondary winding is identical; to the extent that the magnetizing current is small, the secondary turns carry net current $-i(t)$. The windings are surrounded by a magnetic core material that encloses the mutual flux of the transformer.

The high-frequency sinusoidal current $i(t)$ flows on the right surface of primary layer 1, adjacent to layer 2. This induces a copper loss in layer 1, which can be calculated as follows. Let R_{dc} be the dc resistance of layer 1, given by Eq. (13.59), and let I be the rms value of $i(t)$. The skin effect causes the copper loss in layer 1 to be equal to the loss in a conductor of thickness δ with uniform current density. This reduction of the conductor thickness from h to δ effectively increases the resistance by the same factor. Hence, layer 1 can be viewed as having an "ac resistance" given by

$$R_{ac} = \frac{h}{\delta} R_{dc} \tag{13.62}$$

The copper loss in layer 1 is

$$P_1 = I^2 R_{ac} \tag{13.63}$$

The proximity effect causes a current to be induced in the adjacent (left-side) surface of primary layer 2, which tends to oppose the flux generated by the current of layer 1. If the conductors are closely spaced, and if $h \gg \delta$, then the induced current will be equal and opposite to the current $i(t)$, as illustrated

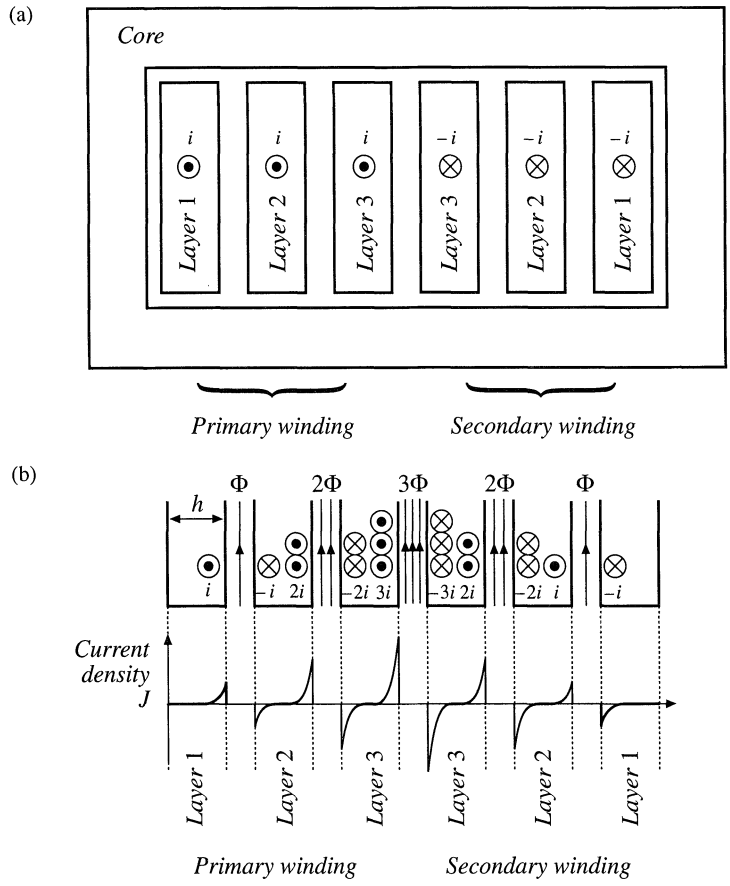

Fig. 13.25 A simple transformer example illustrating the proximity effect: (a) core and winding geometry, (b) distribution of currents on surfaces of conductors.

in Fig. 13.25. Hence, current $-i(t)$ flows on the left surface of the second layer. Since layers 1 and 2 are connected in series, they must both conduct the same net current $i(t)$. As a result, a current $+2i(t)$ must flow on the right-side surface of layer 2.

The current flowing on the left surface of layer 2 has the same magnitude as the current of layer 1, and hence the copper loss is the same: P_1. The current flowing on the right surface of layer 2 has rms magnitude $2I$; hence, it induces copper loss $(2I)^2R_{ac} = 4P_1$. The total copper loss in primary layer 2 is therefore

$$P_2 = P_1 + 4P_1 = 5P_1 \tag{13.64}$$

The copper loss in the second layer is five times as large as the copper loss in the first layer!

The current $2i(t)$ flowing on the right surface of layer 2 induces a flux $2\Phi(t)$ as illustrated in Fig. 13.25. This causes an opposing current $-2i(t)$ to flow on the adjacent (left) surface of primary layer 3. Since layer 3 must also conduct net current $i(t)$, a current $+3i(t)$ flows on the right surface of layer 3. The total copper loss in layer 3 is

$$P_3 = \left(2^2 + 3^2\right)P_1 = 13P_1 \tag{13.65}$$

Likewise, the copper loss in layer m of a multiple-layer winding can be written

$$P_m = I^2\left[(m-1)^2 + m^2\right]\left(\frac{h}{\delta} R_{dc}\right) \tag{13.66}$$

It can be seen that the copper loss compounds very quickly in a multiple-layer winding.

The total copper loss in the three-layer primary winding is $P_1 + 5P_1 + 13P_1$, or $19P_1$. More generally, if the winding contains a total of M layers, then the total copper loss is

$$\begin{aligned} P &= I^2\left(\frac{h}{\delta} R_{dc}\right)\sum_{m=1}^{M}\left[(m-1)^2 + m^2\right] \\ &= I^2\left(\frac{h}{\delta} R_{dc}\right)\frac{M}{3}\left(2M^2 + 1\right) \end{aligned} \tag{13.67}$$

If a dc or low-frequency ac current of rms amplitude I were applied to the M-layer winding, its copper loss would be $P_{dc} = I^2 M R_{dc}$. Hence, the proximity effect increases the copper loss by the factor

$$F_R = \frac{P}{P_{dc}} = \frac{1}{3}\left(\frac{h}{\delta}\right)\left(2M^2 + 1\right) \tag{13.68}$$

This expression is valid for a foil winding having $h \gg \delta$.

As illustrated in Fig. 13.25, the currents in the secondary winding are symmetrical, and hence the secondary winding has the same conduction loss.

The example above, and the associated equations, are limited to $h \gg \delta$ and to the winding geometry shown. The equations do not quantify the behavior for $h \sim \delta$, nor for round conductors, nor are the equations sufficiently general to cover the more complicated winding geometries often encountered in the magnetic devices of switching converters. Optimum designs may, in fact, occur with conductor thicknesses in the vicinity of one penetration depth. The discussions of the following sections allow computation of proximity losses in more general circumstances.

13.4.2 Leakage Flux in Windings

As described above, an externally-applied magnetic field will induce eddy currents to flow in a conductor, and thereby induce copper loss. To understand how magnetic fields are oriented in windings, let us consider the simple two-winding transformer illustrated in Fig. 13.26. In this example, the core has large permeability $\mu \gg \mu_0$. The primary winding consists of eight turns of wire arranged in two layers, and each turn carries current $i(t)$ in the direction indicated. The secondary winding is identical to the primary winding, except that the current polarity is reversed.

Flux lines for typical operation of this transformer are sketched in Fig. 13.26(b). As described in Section 13.2, a relatively large mutual flux is present, which magnetizes the core. In addition, leakage flux is present, which does not completely link both windings. Because of the symmetry of the winding geometry in Fig. 13.26, the leakage flux runs approximately vertically through the windings.

To determine the magnitude of the leakage flux, we can apply Ampere's Law. Consider the closed path taken by one of the leakage flux lines, as illustrated in Fig. 13.27. Since the core has large permeability, we can assume that the MMF induced in the core by this flux is negligible, and that the

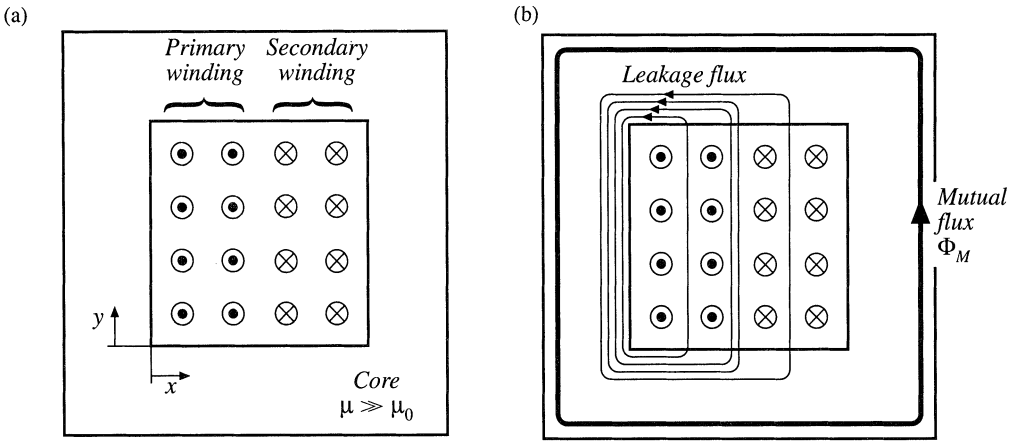

Fig. 13.26 Two-winding transformer example: (a) core and winding geometry, (b) typical flux distribution.

total MMF around the path is dominated by the MMF $\mathcal{F}(x)$ across the core window. Hence, Ampere's Law states that the net current enclosed by the path is equal to the MMF across the air gap:

$$\textit{Enclosed current} = \mathcal{F}(x) = H(x)\ell_w \tag{13.69}$$

where ℓ_w is the height of the window as shown in Fig. 13.27. The net current enclosed by the path depends on the number of primary and secondary conductors enclosed by the path, and is therefore a function of the horizontal position x. The first layer of the primary winding consists of 4 turns, each carrying current $i(t)$. So when the path encloses only the first layer of the primary winding, then the enclosed current is $4i(t)$ as shown in Fig. 13.28. Likewise, when the path encloses both layers of the primary winding, then the enclosed current is $8i(t)$. When the path encloses the entire primary, plus layer 2 of the secondary winding, then the net enclosed current is $8i(t) - 4i(t) = 4i(t)$. The MMF $\mathcal{F}(x)$ across the core window is zero outside the winding, and rises to a maximum of $8i(t)$ at the interface between the primary and secondary windings. Since $H(x) = \mathcal{F}(x)/\ell_w$, the magnetic field intensity $H(x)$ is proportional to the sketch of Fig. 13.28.

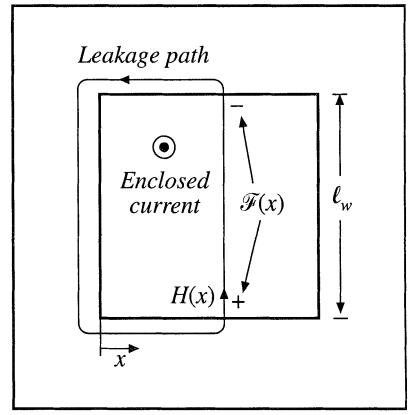

Fig. 13.27 Analysis of leakage flux using Ampere's Law, for the transformer of Fig. 13.26.

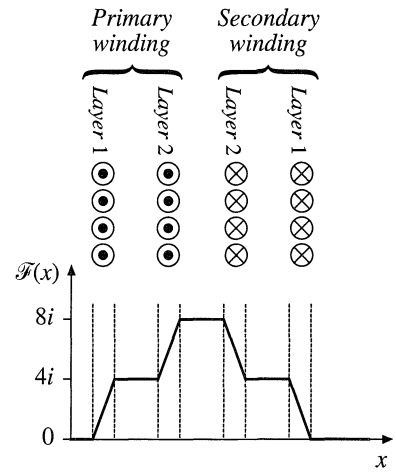

Fig. 13.28 MMF diagram for the transformer winding example of Figs. 13.26 and 13.27.

It should be noted that the shape of the $\mathcal{F}(x)$ curve in the vicinity of the winding conductors depends on the distribution of the current within the conductors. Since this distribution is not yet known, the $\mathcal{F}(x)$ curve of Fig. 13.28 is arbitrarily drawn as straight line segments.

In general, the magnetic fields that surround conductors and lead to eddy currents must be determined using finite element analysis or other similar methods. However, in a large class of coaxial solenoidal winding geometries, the magnetic field lines are nearly parallel to the winding layers. As shown below, we can then obtain an analytical solution for the proximity losses.

13.4.3 Foil Windings and Layers

The winding symmetry described in the previous section allows simplification of the analysis. For the purposes of determining leakage inductance and winding eddy currents, a layer consisting of n_ℓ turns of round wire carrying current $i(t)$ can be approximately modeled as an effective single turn of foil, which carries current $n_\ell i(t)$. The steps in the transformation of a layer of round conductors into a foil conductor are formalized in Fig. 13.29 [6, 8–11]. The round conductors are replaced by square conductors having the same copper cross-sectional area, Fig. 13.29(b). The thickness h of the square conductors is therefore

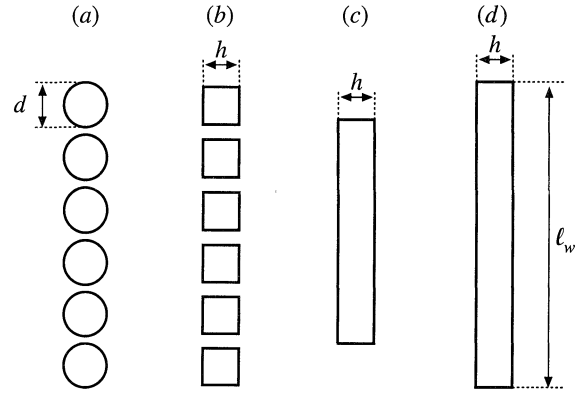

Fig. 13.29 Approximating a layer of round conductors as an effective foil conductor.

equal to the bare copper wire diameter, multiplied by the factor $\sqrt{\pi/4}$:

$$h = \sqrt{\frac{\pi}{4}}\, d \tag{13.70}$$

These square conductors are then joined together, into a foil layer [Fig. 13.29(c)]. Finally, the width of the foil is increased, such that it spans the width of the core window [Fig. 13.29(d)]. Since this stretching process increases the conductor cross-sectional area, a compensating factor η must be introduced such that the correct dc conductor resistance is predicted. This factor, sometimes called the *conductor spacing factor* or the winding *porosity*, is defined as the ratio of the actual layer copper area [Fig. 13.29(a)] to the area of the effective foil conductor of Fig. 13.29(d). The porosity effectively increases the resistivity ρ of the conductor, and thereby increases its skin depth:

$$\delta' = \frac{\delta}{\sqrt{\eta}} \tag{13.71}$$

If a layer of width ℓ_w contains n_ℓ turns of round wire having diameter d, then the winding porosity η is given by

$$\eta = \sqrt{\frac{\pi}{4}}\, d\, \frac{n_\ell}{\ell_w} \tag{13.72}$$

A typical value of η for round conductors that span the width of the winding bobbin is 0.8. In the following analysis, the factor φ is given by h/δ for foil conductors, and by the ratio of the effective foil conductor thickness h to the effective skin depth δ' for round conductors as follows:

$$\varphi = \frac{h}{\delta'} = \sqrt{\eta}\, \sqrt{\frac{\pi}{4}}\, \frac{d}{\delta} \tag{13.73}$$

13.4.4 Power Loss in a Layer

In this section, the average power loss P in a uniform layer of thickness h is determined. As illustrated in Fig. 13.30, the magnetic field strengths on the left and right sides of the conductor are denoted $H(0)$ and $H(d)$, respectively. It is assumed that the component of magnetic field normal to the conductor surface is zero. These magnetic fields are driven by the magnetomotive forces $\mathcal{F}(0)$ and $\mathcal{F}(h)$, respectively. Sinusoidal waveforms are assumed, and rms magnitudes are employed. It is further assumed here that $H(0)$ and $H(h)$ are in phase; the effect of a phase shift is treated in [10].

With these assumptions, Maxwell's equations are solved to find the current density distribution in the layer. The power loss density is then computed, and is integrated over the volume of the layer to find the total copper loss in the layer [10]. The result is

$$P = R_{dc}\, \frac{\varphi}{n_\ell^2} \left[\left(\mathcal{F}^2(h) + \mathcal{F}^2(0) \right) G_1(\varphi) - 4\, \mathcal{F}(h)\, \mathcal{F}(0)\, G_2(\varphi) \right] \tag{13.74}$$

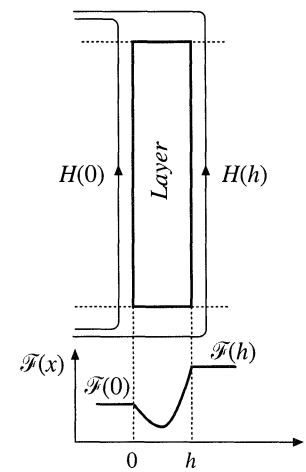

Fig. 13.30 The power loss is determined for a uniform layer. Uniform tangential magnetic fields $H(0)$ and $H(h)$ are applied to the layer surfaces.

where n_ℓ is the number of turns in the layer, and R_{dc} is the dc resistance of the layer. The functions $G_1(\varphi)$ and $G_2(\varphi)$ are

$$G_1(\varphi) = \frac{\sinh(2\varphi) + \sin(2\varphi)}{\cosh(2\varphi) - \cos(2\varphi)}$$
$$G_2(\varphi) = \frac{\sinh(\varphi)\cos(\varphi) + \cosh(\varphi)\sin(\varphi)}{\cosh(2\varphi) - \cos(2\varphi)} \tag{13.75}$$

If the winding carries current of rms magnitude I, then we can write

$$\mathcal{F}(h) - \mathcal{F}(0) = n_\ell I \tag{13.76}$$

Let us further express $\mathcal{F}(h)$ in terms of the winding current I, as

$$\mathcal{F}(h) = m n_\ell I \tag{13.77}$$

The quantity m is therefore the ratio of the MMF $\mathcal{F}(h)$ to the layer ampere-turns $n_\ell I$. Then,

$$\frac{\mathcal{F}(0)}{\mathcal{F}(h)} = \frac{m-1}{m} \tag{13.78}$$

The power dissipated in the layer, Eq. (13.74), can then be written

$$P = I^2 R_{dc} \varphi Q'(\varphi, m) \tag{13.79}$$

where

$$Q'(\varphi, m) = \left(2m^2 - 2m + 1\right) G_1(\varphi) - 4m\left(m - 1\right) G_2(\varphi) \tag{13.80}$$

We can conclude that the proximity effect increases the copper loss in the layer by the factor

$$\frac{P}{I^2 R_{dc}} = \varphi Q'(\varphi, m) \tag{13.81}$$

Equation (13.81), in conjunction with the definitions (13.80), (13.77), (13.75), and (13.73), can be plotted using a computer spreadsheet or small computer program. The result is illustrated in Fig. 13.31, for several values of m.

It is illuminating to express the layer copper loss P in terms of the dc power loss $P_{dc}|_{\varphi = 1}$ that would be obtained in a foil conductor having a thickness $\varphi = 1$. This loss is found by dividing Eq. (13.81) by the effective thickness ratio φ:

$$\frac{P}{P_{dc}\big|_{\varphi = 1}} = Q'(\varphi, m) \tag{13.82}$$

Equation (13.82) is plotted in Fig. 13.32. Large copper loss is obtained for small φ simply because the layer is thin and hence the dc resistance of the layer is large. For large m and large φ, the proximity effect leads to large power loss; Eq. (13.66) predicts that $Q'(\varphi, m)$ is asymptotic to $m^2 + (m-1)^2$ for large φ. Between these extremes, there is a value of φ which minimizes the layer copper loss.

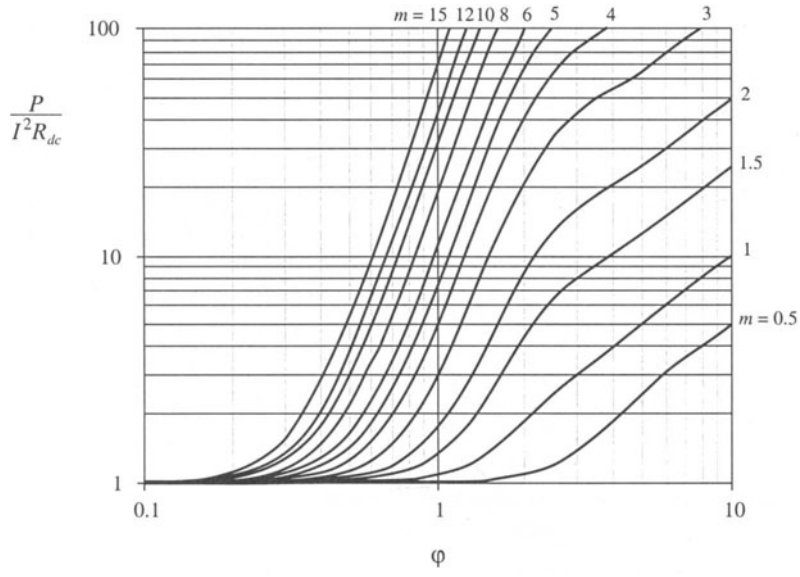

Fig. 13.31 Increase of layer copper loss due to the proximity effect, as a function of φ and MMF ratio m, for sinusoidal excitation.

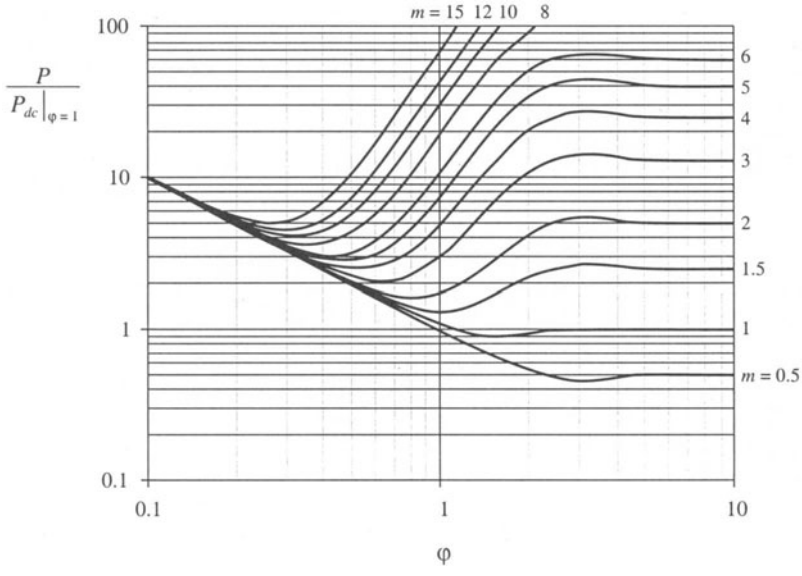

Fig. 13.32 Layer copper loss, relative to the dc loss in a layer having effective thickness of one penetration depth.

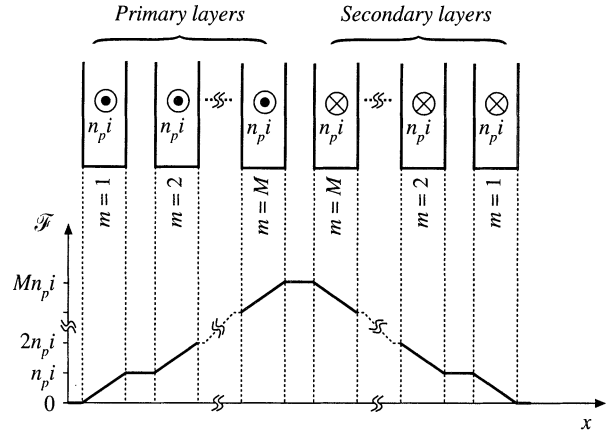

Fig. 13.33 Conventional two-winding transformer example. Each winding consists of M layers.

13.4.5 Example: Power Loss in a Transformer Winding

Let us again consider the proximity loss in a conventional transformer, in which the primary and secondary windings each consist of M layers. The normalized MMF diagram is illustrated in Fig. 13.33. As given by Eq. (13.81), the proximity effect increases the copper loss in each layer by the factor $\varphi Q'(\varphi, m)$. The total increase in primary winding copper loss P_{pri} is found by summation over all of the primary layers:

$$F_R = \frac{P_{pri}}{P_{pri,dc}} = \frac{1}{M} \sum_{m=1}^{M} \varphi Q'(\varphi, m) \tag{13.83}$$

Owing to the symmetry of the windings in this example, the secondary winding copper loss is increased by the same factor. Upon substituting Eq. (13.80) and collecting terms, we obtain

$$F_R = \frac{\varphi}{M} \sum_{m=1}^{M} \left[m^2 \left(2G_1(\varphi) - 4G_2(\varphi) \right) - m \left(2G_1(\varphi) - 4G_2(\varphi) \right) + G_1(\varphi) \right] \tag{13.84}$$

The summation can be expressed in closed form with the help of the identities

$$\begin{aligned} \sum_{m=1}^{M} m &= \frac{M(M+1)}{2} \\ \sum_{m=1}^{M} m^2 &= \frac{M(M+1)(2M+1)}{6} \end{aligned} \tag{13.85}$$

Use of these identities to simplify Eq. (13.84) leads to

$$F_R = \varphi \left[G_1(\varphi) + \frac{2}{3} \left(M^2 - 1 \right) \left(G_1(\varphi) - 2G_2(\varphi) \right) \right] \tag{13.86}$$

This expression is plotted in Fig. 13.34, for several values of M. For large φ, $G_1(\varphi)$ tends to 1, while

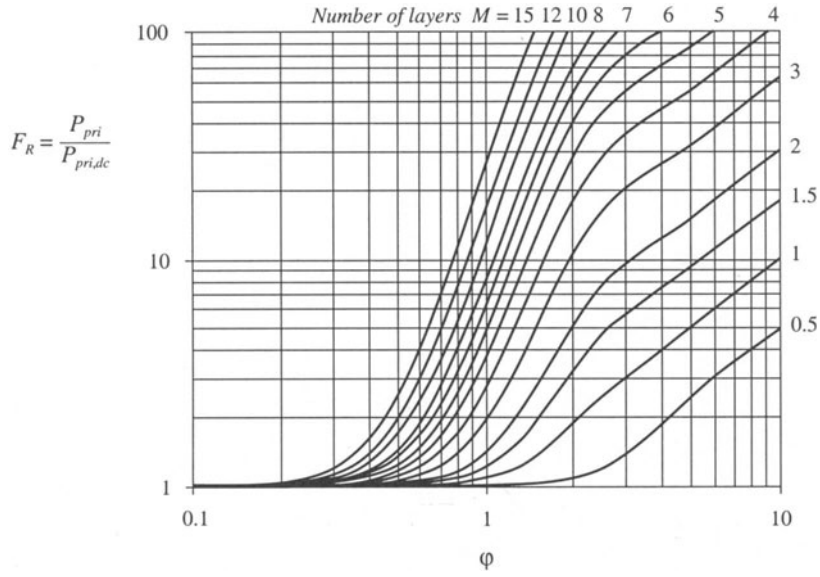

Fig. 13.34 Increased total winding copper loss in the two-winding transformer example, as a function of φ and number of layers M, for sinusoidal excitation.

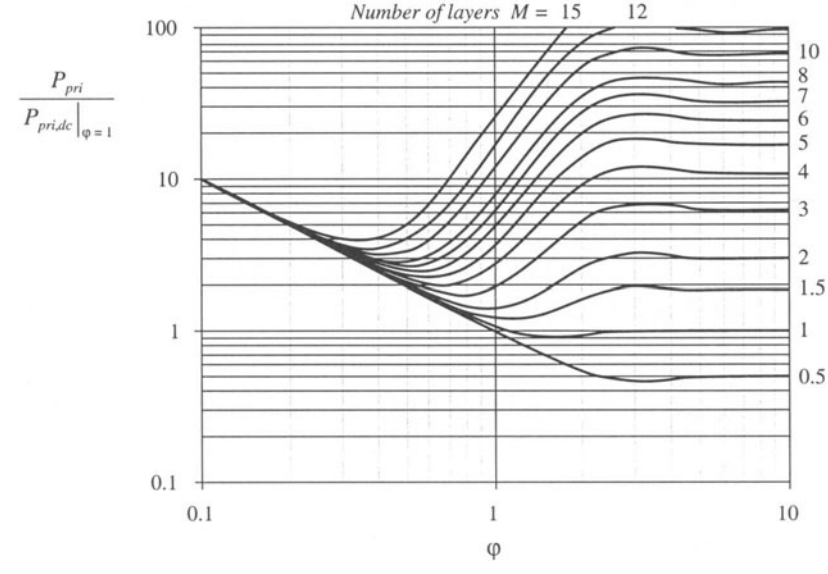

Fig. 13.35 Transformer example winding total copper loss, relative to the winding dc loss for layers having effective thicknesses of one penetration depth.

$G_2(\varphi)$ tends to 0. It can be verified that F_R then tends to the value predicted by Eq. (13.68).

We can again express the total primary power loss in terms of the dc power loss that would be obtained using a conductor in which $\varphi = 1$. This loss is found by dividing Eq. (13.86) by φ:

$$\frac{P_{pri}}{P_{pri,dc}\big|_{\varphi=1}} = G_1(\varphi) + \frac{2}{3}\left(M^2 - 1\right)\left(G_1(\varphi) - 2G_2(\varphi)\right) \tag{13.87}$$

This expression is plotted in Fig. 13.35, for several values of M. Depending on the number of layers, the minimum copper loss for sinusoidal excitation is obtained for φ near to, or somewhat less than, unity.

13.4.6 Interleaving the Windings

One way to reduce the copper losses due to the proximity effect is to interleave the windings. Figure 13.36 illustrates the MMF diagram for a simple transformer in which the primary and secondary layers are alternated, with net layer current of magnitude i. It can be seen that each layer operates with $\mathscr{F} = 0$ on one side, and $\mathscr{F} = i$ on the other. Hence, each layer operates effectively with $m = 1$. Note that Eq. (13.74) is symmetric with respect to $\mathscr{F}(0)$ and $\mathscr{F}(h)$; hence, the copper losses of the interleaved secondary and primary layers are identical. The proximity losses of the entire winding can therefore be determined directly from Fig. 13.34 and 13.35, with $M = 1$. It can be shown that the minimum copper loss for this case (with sinusoidal currents) occurs with $\varphi = \pi/2$, although the copper loss is nearly constant for any $\varphi \geq 1$, and is approximately equal to the dc copper loss obtained when $\varphi = 1$. It should be apparent that interleaving can lead to significant improvements in copper loss when the winding contains several layers.

Partial interleaving can lead to a partial improvement in proximity loss. Figure 13.37 illustrates a transformer having three primary layers and four secondary layers. If the total current carried by each primary layer is $i(t)$, then each secondary layer should carry current $0.75i(t)$. The maximum MMF again occurs in the spaces between the primary and secondary windings, but has value $1.5i(t)$.

To determine the value for m in a given layer, we can solve Eq. (13.78) for m:

$$m = \frac{\mathscr{F}(h)}{\mathscr{F}(h) - \mathscr{F}(0)} \tag{13.88}$$

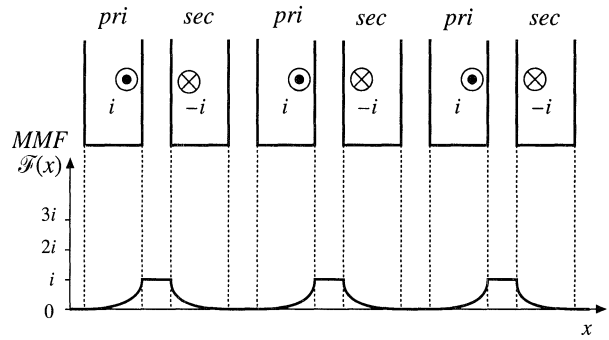

Fig. 13.36 MMF diagram for a simple transformer with interleaved windings. Each layer operates with $m = 1$.

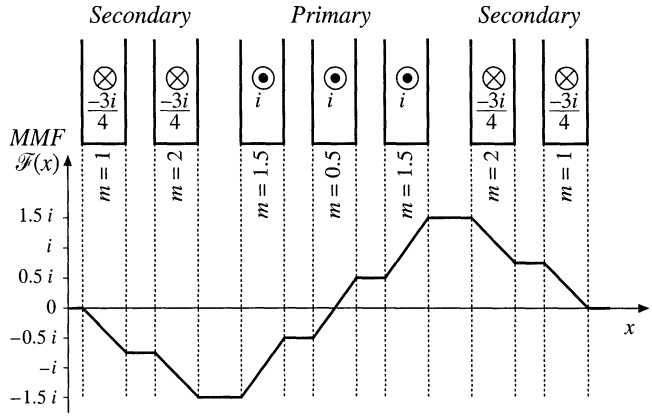

Fig. 13.37 A partially interleaved two-winding transformer, illustrating fractional values of m. The MMF diagram is constructed for the low-frequency limit.

The above expression is valid in general, and Eq. (13.74) is symmetrical in $\mathcal{F}(0)$ and $\mathcal{F}(h)$. However, when $F(0)$ is greater in magnitude than $\mathcal{F}(h)$, it is convenient to interchange the roles of $\mathcal{F}(0)$ and $\mathcal{F}(h)$, so that the plots of Figs. 13.31 and 13.32 can be employed.

In the leftmost secondary layer of Fig. 13.37, the layer carries current $-0.75i$. The MMF changes from 0 to $-0.75i$. The value of m for this layer is found by evaluation of Eq. (13.88):

$$m = \frac{\mathcal{F}(h)}{\mathcal{F}(h) - \mathcal{F}(0)} = \frac{-0.75i}{-0.75i - 0} = 1 \tag{13.89}$$

The loss in this layer, relative to the dc loss of this secondary layer, can be determined using the plots of Figs. 13.31 and 13.32 with $m = 1$. For the next secondary layer, we obtain

$$m = \frac{\mathcal{F}(h)}{\mathcal{F}(h) - \mathcal{F}(0)} = \frac{-1.5i}{-1.5i - (-0.75i)} = 2 \tag{13.90}$$

Hence the loss in this layer can be determined using the plots of Figs. 13.31 and 13.32 with $m = 2$.The next layer is a primary-winding layer. Its value of m can be expressed as

$$m = \frac{\mathcal{F}(0)}{\mathcal{F}(0) - \mathcal{F}(h)} = \frac{-1.5i}{-1.5i - (-0.5i)} = 1.5 \tag{13.91}$$

The loss in this layer, relative to the dc loss of this primary layer, can be determined using the plots of Figs. 13.31 and 13.32 with $m = 1.5$. The center layer has an m of

$$m = \frac{\mathcal{F}(h)}{\mathcal{F}(h) - \mathcal{F}(0)} = \frac{0.5i}{0.5i - (-0.5i)} = 0.5 \tag{13.92}$$

The loss in this layer, relative to the dc loss of this primary layer, can be determined using the plots of Figs. 13.31 and 13.32 with $m = 0.5$. The remaining layers are symmetrical to the corresponding layers described above, and have identical copper losses. The total loss in the winding is found by summing the losses described above for each layer.

Interleaving windings can significantly reduce the proximity loss when the primary and secondary currents are in phase. However, in some cases such as the transformers of the flyback and SEPIC converters, the winding currents are out of phase. Interleaving then does little to reduce the MMFs and magnetic fields in the vicinity of the windings, and hence the proximity loss is essentially unchanged. It should also be noted that Eqs. (13.74) to (13.82) assume that the winding currents are in phase. General expressions for out-of-phase currents, as well as analysis of a flyback example, are given in [10].

The above procedure can be used to determine the high-frequency copper losses of more complicated multiple-winding magnetic devices. The MMF diagrams are constructed, and then the power loss in each layer is evaluated using Eq. (13.81). These losses are summed, to find the total copper loss. The losses induced in electrostatic shields can also be determined. Several additional examples are given in [10].

It can be concluded that, for sinusoidal currents, there is an optimal conductor thickness in the vicinity of $\varphi = 1$ that leads to minimum copper loss. It is highly advantageous to minimize the number of layers, and to interleave the windings. The amount of copper in the vicinity of the high-MMF portions of windings should be kept to a minimum. Core geometries that maximize the width ℓ_w of the layers, while minimizing the overall number of layers, lead to reduced proximity loss.

Use of *Litz* wire is another means of increasing the conductor area while maintaining low proximity losses. Tens, hundreds, or more strands of small-gauge insulated copper wire are bundled together, and are externally connected in parallel. These strands are twisted, or transposed, such that each strand passes equally through each position inside and on the surface of the bundle. This prevents the circulation of high-frequency currents between strands. To be effective, the diameter of the strands should be sufficiently less than one skin depth. Also, it should be pointed out that the Litz wire bundle itself is composed of multiple layers. The disadvantages of Litz wire are its increased cost, and its reduced fill factor.

13.4.7 PWM Waveform Harmonics

The pulse-width-modulated waveforms encountered in switching converters contain significant harmonics, which can lead to increased proximity losses. The effect of harmonics on the losses in a layer can be determined via field harmonic analysis [10], in which the MMF waveforms $\mathscr{F}(0,t)$ and $\mathscr{F}(d,t)$ of Eq. (13.74) are expressed in Fourier series. The power loss of each individual harmonic is computed as in Section 13.4.4, and the losses are summed to find the total loss in a layer. For example, the PWM waveform of Fig. 13.38 can be represented by the following Fourier series:

$$i(t) = I_0 + \sum_{j=1}^{\infty} \sqrt{2}\, I_j \cos(j\omega t) \tag{13.93}$$

where

$$I_j = \frac{\sqrt{2}\, I_{pk}}{j\pi} \sin(j\pi D)$$

with $\omega = 2\pi/T_s$. This waveform contains a dc component $I_0 = DI_{pk}$, plus harmonics of rms magnitude I_j proportional to $1/j$. The transformer winding current waveforms of most switching converters follow this Fourier series, or a similar series.

Effects of waveforms harmonics on proximity losses are discussed in [8–10]. The dc component of the winding currents does not lead to proximity loss, and should not be included in proximity loss calculations. Failure to remove the dc component can lead to significantly pessimistic estimates of copper

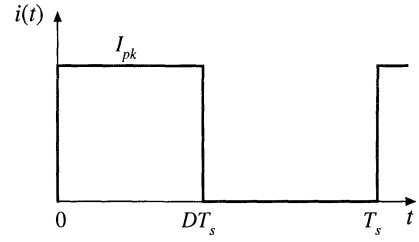

Fig. 13.38 Pulse-width modulated winding current waveform.

loss. The skin depth δ is smaller for high frequency harmonics than for the fundamental, and hence the waveform harmonics exhibit an increased effective φ. Let φ_1 be given by Eq. (13.73), in which δ is found by evaluation of Eq. (13.60) at the fundamental frequency. Since the penetration depth δ varies as the inverse square-root of frequency, the effective value of φ for harmonic j is

$$\varphi_j = \sqrt{j}\,\varphi_1 \tag{13.94}$$

In a multiple-layer winding excited by a current waveform whose fundamental component has $\varphi = \varphi_1$ close to 1, harmonics can significantly increase the total copper loss. This occurs because, for $m > 1$, $Q'(\varphi, m)$ is a rapidly increasing function of φ in the vicinity of 1. When φ_1 is sufficiently greater than 1, then $Q'(\varphi, m)$ is nearly constant, and harmonics have less influence on the total copper loss.

For example, suppose that the two-winding transformer of Fig. 13.33 is employed in a converter such as the forward converter, in which a winding current waveform $i(t)$ can be well approximated by the Fourier series of Eq. (13.93). The winding contains M layers, and has dc resistance R_{dc}. The copper loss induced by the dc component is

$$P_{dc} = I_0^2 R_{dc} \tag{13.95}$$

The copper loss P_j ascribable to harmonic j is found by evaluation of Eq. (13.86) with $\varphi = \varphi_j$:

$$P_j = I_j^2 R_{dc} \sqrt{j}\,\varphi_1 \left[G_1(\sqrt{j}\,\varphi_1) + \frac{2}{3}\left(M^2 - 1\right)\left(G_1(\sqrt{j}\,\varphi_1) - 2G_2(\sqrt{j}\,\varphi_1)\right) \right] \tag{13.96}$$

The total copper loss in the winding is the sum of losses arising from all components of the harmonic series:

$$\frac{P_{cu}}{DI_{pk}^2 R_{dc}} = D + \frac{2\varphi_1}{D\pi^2} \sum_{j=1}^{\infty} \frac{\sin^2(j\pi D)}{j\sqrt{j}} \left[G_1(\sqrt{j}\,\varphi_1) + \frac{2}{3}\left(M^2 - 1\right)\left(G_1(\sqrt{j}\,\varphi_1) - 2G_2(\sqrt{j}\,\varphi_1)\right) \right] \tag{13.97}$$

In Eq. (13.97), the copper loss is expressed relative to the loss $DI_{pk}^2 R_{dc}$ predicted by a low-frequency analysis. This expression can be evaluated by use of a computer program or computer spreadsheet.

To explicitly quantify the effects of harmonics, we can define the harmonic loss factor F_H as

$$F_H = \frac{\sum_{j=1}^{\infty} P_j}{P_1} \tag{13.98}$$

with P_j given by Eq. (13.96). The total winding copper loss is then given by

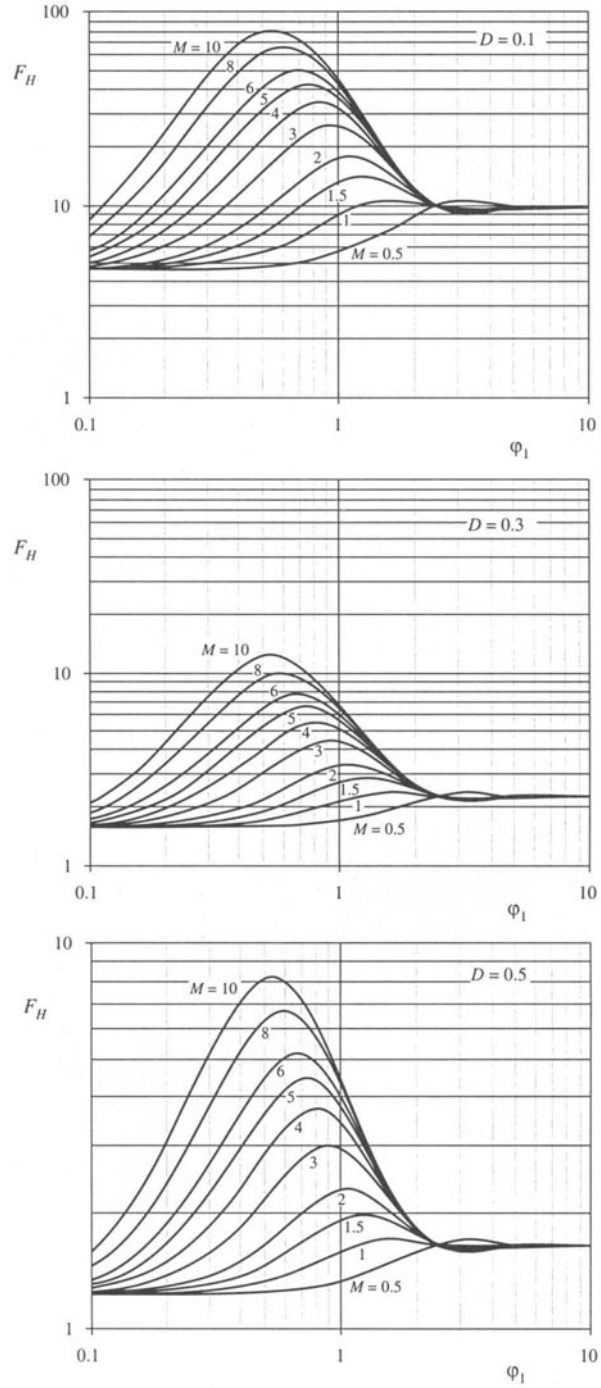

Fig. 13.39 Increased proximity losses induced by PWM waveform harmonics, forward converter example: (a) at $D = 0.1$, (b) at $D = 0.3$, (c) at $D = 0.5$.

$$P_{cu} = I_0^2 R_{dc} + F_H F_R I_1^2 R_{dc} \tag{13.99}$$

with F_R given by Eq. (13.86). The harmonic factor F_H is a function not only of the winding geometry, but also of the harmonic spectrum of the winding current waveform. The harmonic factor F_H is plotted in Fig. 13.39 for several values of D, for the simple transformer example. The total harmonic distortion (THD) of the example current waveforms are: 48% for $D = 0.5$, 76% for $D = 0.3$, and 191% for $D = 0.1$. The waveform THD is defined as

$$\text{THD} = \frac{\sqrt{\sum_{j=2}^{\infty} I_j^2}}{I_1} \tag{13.100}$$

It can be seen that harmonics significantly increase the proximity loss of a multilayer winding when φ_1 is close to 1. For sufficiently small φ_1, the proximity effect can be neglected, and F_H tends to the value $1 + (\text{THD})^2$. For large φ_1, the harmonics also increase the proximity loss; however, the increase is less dramatic than for φ_1 near 1 because the fundamental component proximity loss is large. It can be concluded that, when the current waveform contains high THD and when the winding contains several layers or more, then proximity losses can be kept low only by choosing φ_1 much less than 1. Interleaving the windings allows a larger value of φ_1 to be employed.

13.5 SEVERAL TYPES OF MAGNETIC DEVICES, THEIR *B–H* LOOPS, AND CORE VS. COPPER LOSS

A variety of magnetic elements are commonly used in power applications, which employ the properties of magnetic core materials and windings in different ways. As a result, quite a few factors constrain the design of a magnetic device. The maximum flux density must not saturate the core. The peak ac flux density should also be sufficiently small, such that core losses are acceptably low. The wire size should be sufficiently small, to fit the required number of turns in the core window. Subject to this constraint, the wire cross-sectional area should be as large as possible, to minimize the winding dc resistance and copper loss. But if the wire is too thick, then unacceptable copper losses occur owing to the proximity effect. An air gap is needed when the device stores significant energy. But an air gap is undesirable in transformer applications. It should be apparent that, for a given magnetic device, some of these constraints are active while others are not significant.

Thus, design of a magnetic element involves not only obtaining the desired inductance or turns ratio, but also ensuring that the core material does not saturate and that the total power loss is not too large. Several common power applications of magnetics are discussed in this section, which illustrate the factors governing the choice of core material, maximum flux density, and design approach.

13.5.1 Filter Inductor

A filter inductor employed in a CCM buck converter is illustrated in Fig. 13.40(a). In this application, the value of inductance L is usually chosen such that the inductor current ripple peak magnitude Δi is a small fraction of the full-load inductor current dc component I, as illustrated in Fig. 13.40(b). As illustrated in Fig. 13.41, an air gap is employed that is sufficiently large to prevent saturation of the core by the peak current $I + \Delta i$.

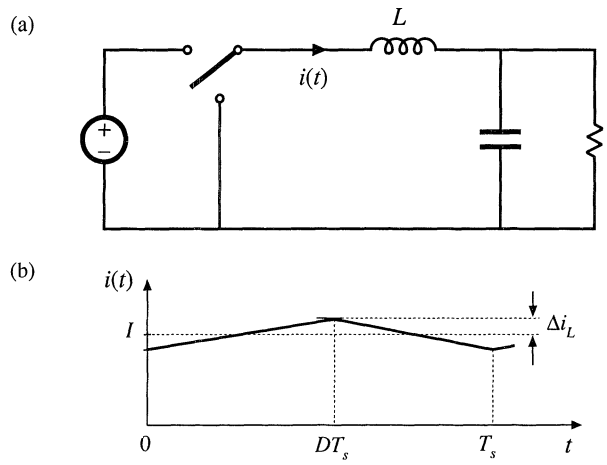

Fig. 13.40 Filter inductor employed in a CCM buck converter: (a) circuit schematic, (b) inductor current waveform.

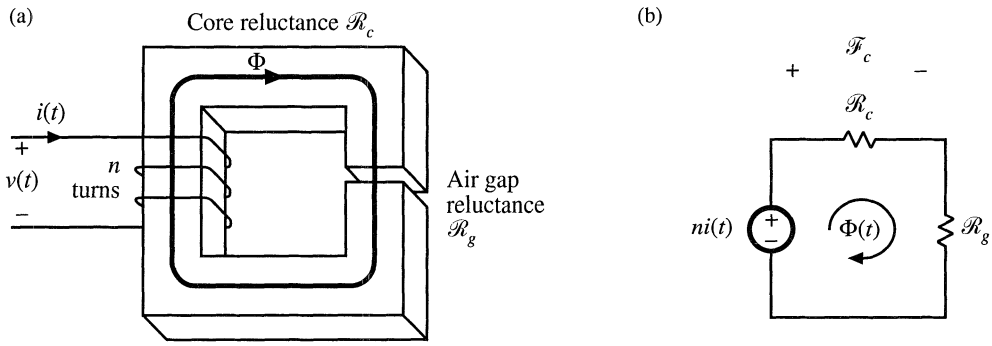

Fig. 13.41 Filter inductor: (a) structure, (b) magnetic circuit model.

The core magnetic field strength $H_c(t)$ is related to the winding current $i(t)$ according to

$$H_c(t) = \frac{ni(t)}{\ell_c} \frac{\mathcal{R}_c}{\mathcal{R}_c + \mathcal{R}_g} \tag{13.101}$$

where ℓ_c is the magnetic path length of the core. Since $H_c(t)$ is proportional to $i(t)$, $H_c(t)$ can be expressed as a large dc component H_{c0} and a small superimposed ac ripple ΔH_c, where

$$\begin{aligned} H_{c0} &= \frac{nI}{\ell_c} \frac{\mathcal{R}_c}{\mathcal{R}_c + \mathcal{R}_g} \\ \Delta H_c &= \frac{n\Delta i}{\ell_c} \frac{\mathcal{R}_c}{\mathcal{R}_c + \mathcal{R}_g} \end{aligned} \tag{13.102}$$

A sketch of $B(t)$ vs. $H_c(t)$ for this application is given in Fig. 13.42. This device operates with the minor B–H loop illustrated. The size of the minor loop, and hence the core loss, depends on the magnitude of the inductor current ripple Δi. The copper loss depends on the rms inductor current ripple, essentially

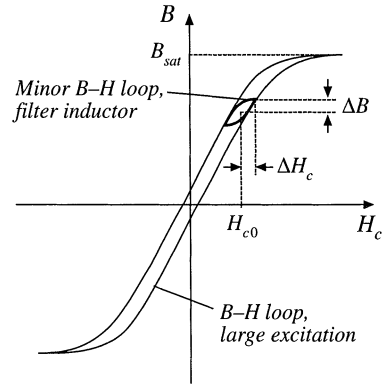

Fig. 13.42 Filter inductor minor *B–H* loop.

equal to the dc component *I*. Typically, the core loss can be ignored, and the design is driven by the copper loss. The maximum flux density is limited by saturation of the core. Proximity losses are negligible. Although a high-frequency ferrite material can be employed in this application, other materials having higher core losses and greater saturation flux density lead to a physically smaller device. Design of a filter inductor in which the maximum flux density is a specified value is considered in the next chapter.

13.5.2 AC Inductor

An ac inductor employed in a resonant converter is illustrated in Fig. 13.43. In this application, the high-frequency current variations are large. In consequence, the $B(t)$–$H(t)$ loop illustrated in Fig. 13.44 is large. Core loss and proximity loss are usually significant in this application. The maximum flux density

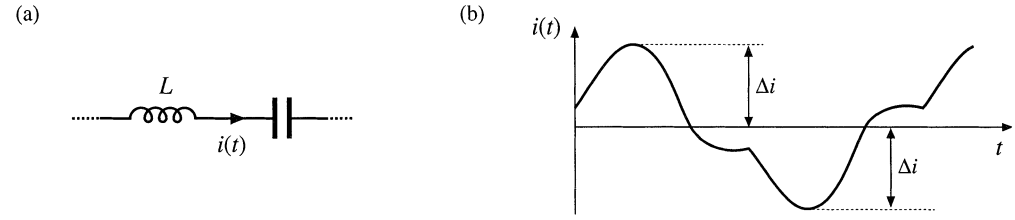

Fig. 13.43 Ac inductor, resonant converter example: (a) resonant tank circuit, (b) inductor current waveform.

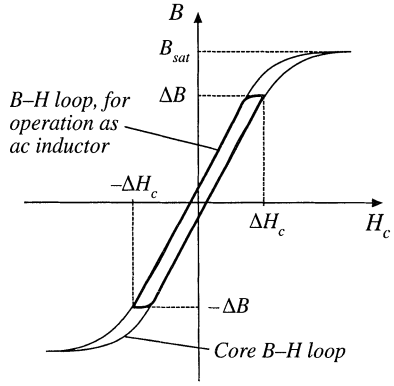

Fig. 13.44 Operational *B–H* loop of an ac inductor.

is limited by core loss rather than saturation. Both core loss and copper loss must be accounted for in the design of this element, and the peak ac flux density ΔB is a design variable that is typically chosen to minimize the total loss. A high-frequency material having low core loss, such as ferrite, is normally employed. Design of magnetics such as this, in which the ac flux density is a design variable that is chosen in a optimal manner, is considered in Chapter 15.

13.5.3 Transformer

Figure 13.45 illustrates a conventional transformer employed in a switching converter. Magnetization of the core is modeled by the magnetizing inductance L_M. The magnetizing current $i_M(t)$ is related to the core magnetic field $H(t)$ according to Ampere's law

$$H(t) = \frac{ni_M(t)}{\ell_m} \tag{13.103}$$

However, $i_M(t)$ is not a direct function of the winding currents $i_1(t)$ or $i_2(t)$. Rather, the magnetizing current is dependent on the applied winding voltage waveform $v_1(t)$. Specifically, the maximum ac flux density is directly proportional to the applied volt-seconds λ_1. A typical B–H loop for this application is illustrated in Fig. 13.46.

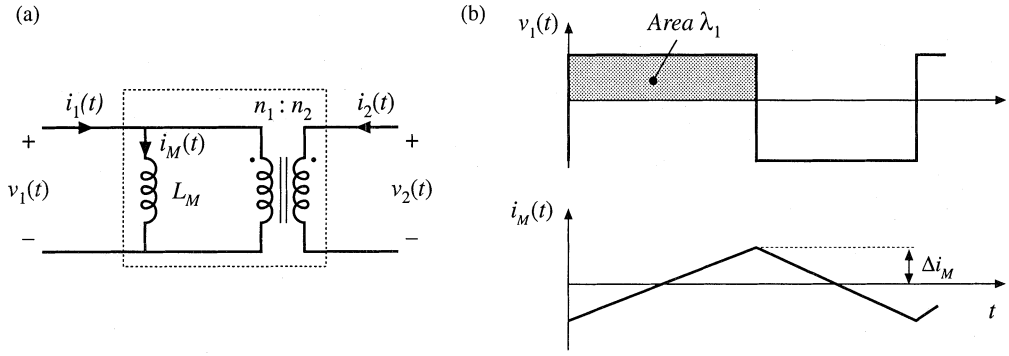

Fig. 13.45 Conventional transformer: (a) equivalent circuit, (b) typical primary voltage and magnetizing current waveforms.

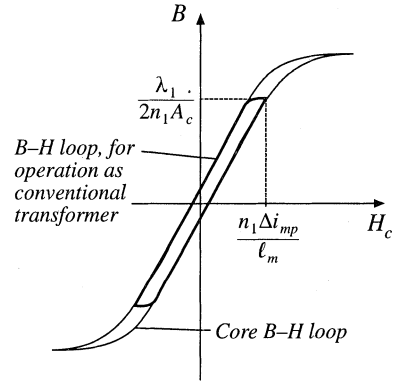

Fig. 13.46 Operational B–H loop of a conventional transformer.

In the transformer application, core loss and proximity losses are usually significant. Typically the maximum flux density is limited by core loss rather than by saturation. A high-frequency material having low core loss is employed. Both core and copper losses must be accounted for in the design of the transformer. The design must also incorporate multiple windings. Transformer design with flux density optimized for minimum total loss is described in Chapter 15.

13.5.4 Coupled Inductor

A coupled inductor is a filter inductor having multiple windings. Figure 13.47(a) illustrates coupled inductors in a two-output forward converter. The inductors can be wound on the same core, because the winding voltage waveforms are proportional. The inductors of the SEPIC and Ćuk converters, as well as of multiple-output buck-derived converters and some other converters, can be coupled. The inductor current ripples can be controlled by control of the winding leakage inductances [12,13]. Dc currents flow in each winding as illustrated in Fig. 13.47(b), and the net magnetization of the core is proportional to the sum of the winding ampere-turns:

$$H_c(t) = \frac{n_1 i_1(t) + n_2 i_2(t)}{\ell_c} \frac{\mathcal{R}_c}{\mathcal{R}_c + \mathcal{R}_g} \tag{13.104}$$

As in the case of the single-winding filter inductor, the size of the minor *B–H* loop is proportional to the total current ripple (Fig. 13.48). Small ripple implies small core loss, as well as small proximity loss. An air gap is employed, and the maximum flux density is typically limited by saturation.

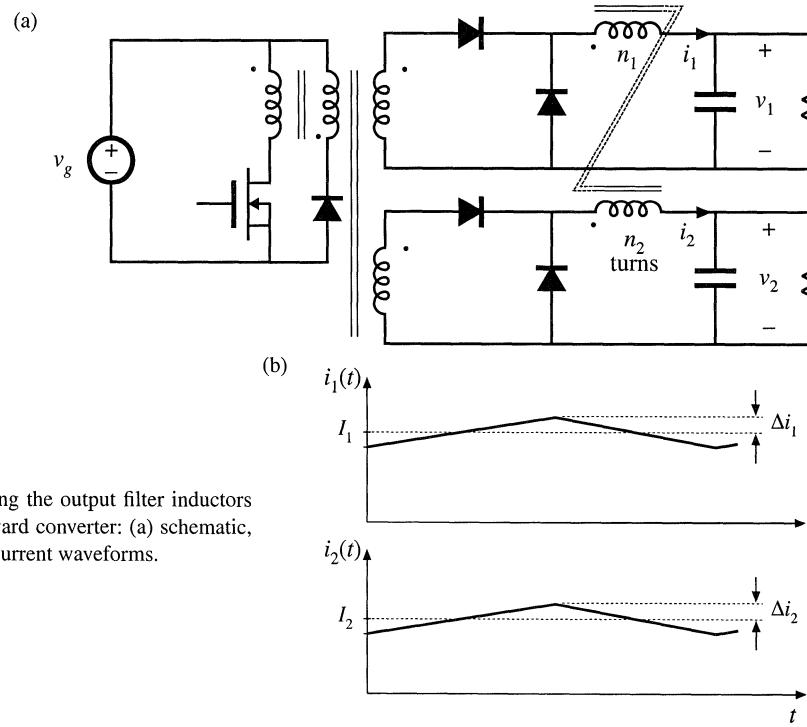

Fig. 13.47 Coupling the output filter inductors of a two-output forward converter: (a) schematic, (b) typical inductor current waveforms.

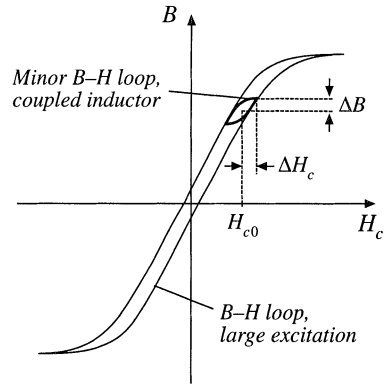

Fig. 13.48 Coupled inductor minor *B–H* loop.

13.5.5 Flyback Transformer

As discussed in Chapter 6, the flyback transformer functions as an inductor with two windings. The primary winding is used during the transistor conduction interval, and the secondary is used during the diode conduction interval. A flyback converter is illustrated in Fig. 13.49(a), with the flyback transformer modeled as a magnetizing inductance in parallel with an ideal transformer. The magnetizing current $i_M(t)$ is proportional to the core magnetic field strength $H_c(t)$. Typical DCM waveforms are given in Fig. 13.49(b).

Since the flyback transformer stores energy, an air gap is needed. Core loss depends on the magnitude of the ac component of the magnetizing current. The *B–H* loop for discontinuous conduction mode operation is illustrated in Fig. 13.50. When the converter is designed to operate in DCM, the core loss is significant. The peak ac flux density ΔB is then chosen to maintain an acceptably low core loss. For CCM operation, core loss is less significant, and the maximum flux density may be limited only by saturation of the core. In either case, winding proximity losses are typically quite significant. Unfortunately, interleaving the windings has little impact on the proximity loss because the primary and secondary winding currents are out of phase.

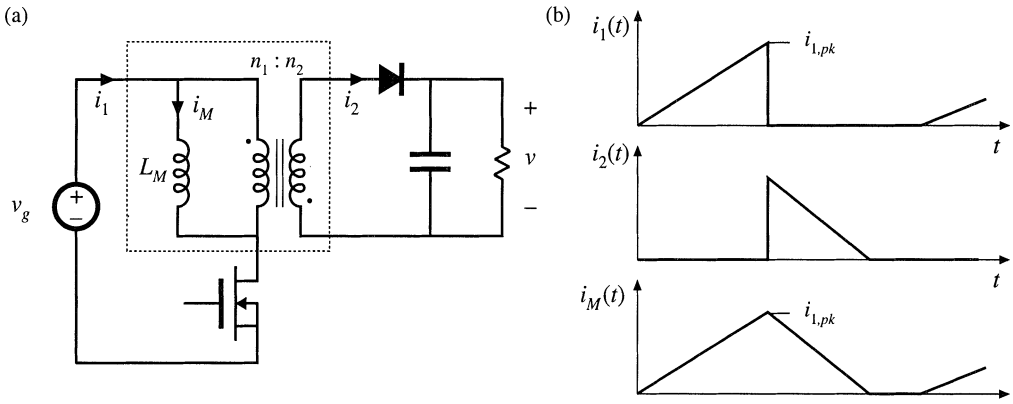

Fig. 13.49 Flyback transformer: (a) converter schematic, with transformer equivalent circuit, (b) DCM current waveforms.

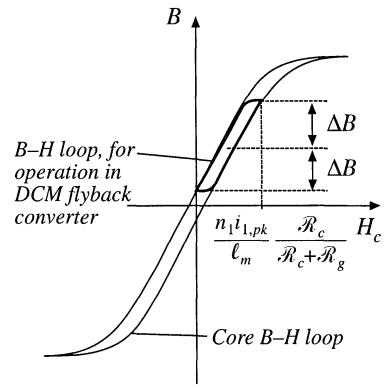

Fig. 13.50 Operational *B–H* loop of a DCM flyback transformer.

13.6 SUMMARY OF KEY POINTS

1. Magnetic devices can be modeled using lumped-element magnetic circuits, in a manner similar to that commonly used to model electrical circuits. The magnetic analogs of electrical voltage V, current I, and resistance R, are magnetomotive force (MMF) $\mathcal{F}$, flux Φ, and reluctance $\mathcal{R}$ respectively.

2. Faraday's law relates the voltage induced in a loop of wire to the derivative of flux passing through the interior of the loop.

3. Ampere's law relates the total MMF around a loop to the total current passing through the center of the loop. Ampere's law implies that winding currents are sources of MMF, and that when these sources are included, then the net MMF around a closed path is equal to zero.

4. Magnetic core materials exhibit hysteresis and saturation. A core material saturates when the flux density B reaches the saturation flux density B_{sat}.

5. Air gaps are employed in inductors to prevent saturation when a given maximum current flows in the winding, and to stabilize the value of inductance. The inductor with air gap can be analyzed using a simple magnetic equivalent circuit, containing core and air gap reluctances and a source representing the winding MMF.

6. Conventional transformers can be modeled using sources representing the MMFs of each winding, and the core MMF. The core reluctance approaches zero in an ideal transformer. Nonzero core reluctance leads to an electrical transformer model containing a magnetizing inductance, effectively in parallel with the ideal transformer. Flux that does not link both windings, or "leakage flux," can be modeled using series inductors.

7. The conventional transformer saturates when the applied winding volt-seconds are too large. Addition of an air gap has no effect on saturation. Saturation can be prevented by increasing the core cross-sectional area, or by increasing the number of primary turns.

8. Magnetic materials exhibit core loss, due to hysteresis of the *B–H* loop and to induced eddy currents flowing in the core material. In available core materials, there is a tradeoff between high saturation flux density B_{sat} and high core loss P_{fe}. Laminated iron alloy cores exhibit the highest B_{sat} but also the highest P_{fe}, while ferrite cores exhibit the lowest P_{fe} but also the lowest B_{sat}. Between these two extremes are powdered iron alloy and amorphous alloy materials.

9. The skin and proximity effects lead to eddy currents in winding conductors, which increase the copper loss P_{cu} in high-current high-frequency magnetic devices. When a conductor has thickness approaching or

larger than the penetration depth δ, magnetic fields in the vicinity of the conductor induce eddy currents in the conductor. According to Lenz's law, these eddy currents flow in paths that tend to oppose the applied magnetic fields.

10. The magnetic field strengths in the vicinity of the winding conductors can be determined by use of MMF diagrams. These diagrams are constructed by application of Ampere's law, following the closed paths of the magnetic field lines which pass near the winding conductors. Multiple-layer noninterleaved windings can exhibit high maximum MMFs, with resulting high eddy currents and high copper loss.

11. An expression for the copper loss in a layer, as a function of the magnetic field strengths or MMFs surrounding the layer, is given in Section 13.4.4. This expression can be used in conjunction with the MMF diagram, to compute the copper loss in each layer of a winding. The results can then be summed, yielding the total winding copper loss. When the effective layer thickness is near to or greater than one skin depth, the copper losses of multiple-layer noninterleaved windings are greatly increased.

12. Pulse-width-modulated winding currents contain significant total harmonic distortion, which can lead to a further increase of copper loss. The increase in proximity loss caused by current harmonics is most pronounced in multiple-layer non-interleaved windings, with an effective layer thickness near one skin depth.

REFERENCES

[1] MIT STAFF, *Magnetic Circuits and Transformers*, Cambridge: The MIT Press, 1943.

[2] J. K. WATSON, *Applications of Magnetism*, New York: John Wiley & Sons, 1980.

[3] R. P. SEVERNS and G. E. BLOOM, *Modern Dc-to-Dc Switchmode Power Converter Circuits*, New York: Van Nostrand Reinhold, 1985.

[4] A. DAUHAJRE and R. D. MIDDLEBROOK, "Modeling and Estimation of Leakage Phenomena in Magnetic Circuits," *IEEE Power Electronics Specialists Conference*, 1986 Record, pp. 213-226.

[5] S. EL-HAMAMSY and E. CHANG, "Magnetics Modeling for Computer-Aided Design of Power Electronics Circuits," *IEEE Power Electronics Specialists Conference*, 1989 Record, pp. 635-645.

[6] P. L. DOWELL, "Effects of Eddy Currents in Transformer Windings," *Proceedings of the IEE*, Vol. 113, No. 8, August 1966, pp. 1387-1394.

[7] M. P. PERRY, "Multiple Layer Series Connected Winding Design for Minimum Loss," *IEEE Transactions on Power Apparatus and Systems*, Vol. PAS-98, No. 1, Jan./Feb. 1979, pp. 116-123.

[8] P. S. VENKATRAMAN, "Winding Eddy Current Losses in Switch Mode Power Transformers Due to Rectangular Wave Currents," *Proceedings of Powercon 11*, 1984, pp. A1.1 - A1.11.

[9] B. CARSTEN, "High Frequency Conductor Losses in Switchmode Magnetics," *High Frequency Power Converter Conference*, 1986 Record, pp. 155-176.

[10] J. P. VANDELAC and P. ZIOGAS, "A Novel Approach for Minimizing High Frequency Transformer Copper Losses," *IEEE Power Electronics Specialists Conference*, 1987 Record, pp. 355-367.

[11] A. M. URLING, V. A. NIEMELA, G. R. SKUTT, and T. G. WILSON, "Characterizing High-Frequency Effects in Transformer Windings—A Guide to Several Significant Articles," *IEEE Applied Power Electronics Conference*, 1989 Record, pp. 373-385.

[12] S. ĆUK and R. D. MIDDLEBROOK, "Coupled-Inductor and Other Extensions of a New Optimum Topology Switching Dc–to–Dc Converter," *IEEE Industry Applications Society Annual Meeting*, 1977 Proceedings, pp. 1110-1122.

[13] S. ĆUK and Z. ZHANG, "Coupled-Inductor Analysis and Design," *IEEE Power Electronics Specialists Conference*, 1986 Record, pp. 655-665.

PROBLEMS

13.1 The core illustrated in Fig. 13.51(a) is 1 cm thick. All legs are 1 cm wide, except for the right-hand side vertical leg, which is 0.5 cm wide. You may neglect nonuniformities in the flux distribution caused by turning corners.

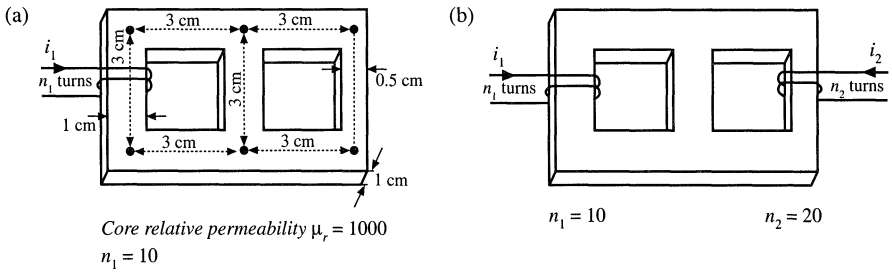

Fig. 13.51 Problem 13.1

(a) Determine the magnetic circuit model of this device, and label the values of all reluctances in your model.

(b) Determine the inductance of the winding.

A second winding is added to the same core, as shown in Fig. 13.51(b).

(c) Modify your model of part (a) to include this winding.

(d) The electrical equations for this circuit may be written in the form

$$\begin{bmatrix} v_1 \\ v_2 \end{bmatrix} = \begin{bmatrix} L_{11} & L_{12} \\ L_{12} & L_{22} \end{bmatrix} \frac{d}{dt} \begin{bmatrix} i_1 \\ i_2 \end{bmatrix}$$

Use superposition to determine analytical expressions and numerical values for L_{11}, L_{12}, and L_{22}.

13.2 Two windings are placed as illustrated in Fig. 13.52(a) on a core of uniform cross-sectional area $A_c = 1$ cm^2. Each winding has 50 turns. The relative permeability of the core is $\mu_r = 10^4$.

(a) Sketch an equivalent magnetic circuit, and determine numerical values for each reluctance.

(b) Determine the self-inductance of each winding.

(c) Determine the inductance L^+ obtained when the windings are connected in series as in Fig. 13.52(b).

(d) Determine the inductance L^- obtained when the windings are connected in anti-series as in Fig. 13.52(c).

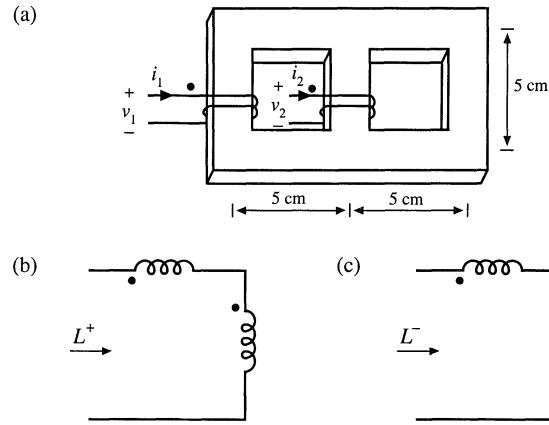

Fig. 13.52 Problem 13.2.

13.3 All three legs of the magnetic device illustrated in Fig. 13.53 are of uniform cross-sectional area A_C. Legs 1 and 2 each have magnetic path length 3ℓ, while leg 3 has magnetic path length ℓ. Both windings have n turns. The core has permeability $\mu \gg \mu_0$.

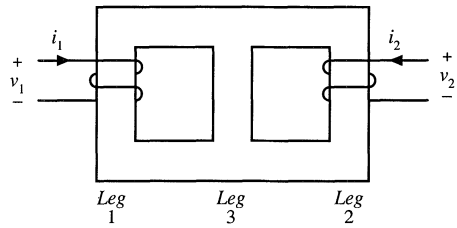

Fig. 13.53 Magnetic core for Problem 13.3.

(a) Sketch a magnetic equivalent circuit, and give analytical expressions for all element values.

A voltage source is connected to winding 1, such that $v_1(t)$ is a square wave of peak value V_{max} and period T_s. Winding 2 is open-circuited.

(b) Sketch $i_1(t)$ and label its peak value.

(c) Find the flux $\varphi_2(t)$ in leg 2. Sketch $\varphi_2(t)$ and label its peak value.

(d) Sketch $v_2(t)$ and label its peak value.

13.4 The magnetic device illustrated in Fig. 13.54(a) consists of two windings, which can replace the two inductors in a Ćuk, SEPIC, or other similar converter. For this problem, all three legs have the same uniform cross-sectional area A_c. The legs have gaps of lengths g_1, g_2, and g_3, respectively. The core permeability μ is very large. You may neglect fringing flux. Legs 1 and 2 have windings containing n_1 and n_2 turns, respectively.

(a) Derive a magnetic circuit model for this device, and give analytical expressions for each reluctance in your model. Label the polarities of the MMF generators.

(b) Write the electrical terminal equations of this device in the matrix form

$$\begin{bmatrix} v_1 \\ v_2 \end{bmatrix} = \begin{bmatrix} L_{11} & L_{12} \\ L_{12} & L_{22} \end{bmatrix} \frac{d}{dt} \begin{bmatrix} i_1 \\ i_2 \end{bmatrix}$$

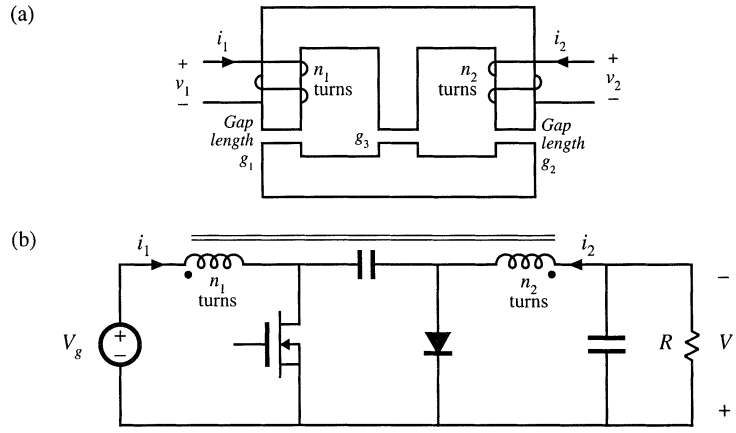

Fig. 13.54 Magnetic core and converter for Problem 13.4.

and derive analytical expressions for L_{11}, L_{12}, and L_{22}.

(c) Derive an electrical circuit model for this device, and give analytical expressions for the turns ratio and each inductance in your model, in terms of the turns and reluctances of part (a).

This single magnetic device is to be used to realize the two inductors of the Ćuk converter, as in Fig. 13.54(b).

(d) Sketch the voltage waveforms $v_1(t)$ and $v_2(t)$, making the linear ripple approximation as appropriate. You may assume that the converter operates in the continuous conduction mode.

(e) The voltage waveforms of part (d) are applied to your model of parts (b) and (c). Solve your model to determine the slopes of the inductor current ripples during intervals DT_s and $D'T_s$. Sketch the steady-state inductor current waveforms $i_1(t)$ and $i_2(t)$, and label all slopes.

(f) By skillful choice of n_1/n_2 and the air gap lengths, it is possible to make the inductor current ripple Δi in either $i_1(t)$ or $i_2(t)$ go to zero. Determine the conditions on n_1/n_2, g_1, g_2, and g_3 that cause the current ripple in $i_2(t)$ to become zero. Sketch the resulting $i_1(t)$ and $i_2(t)$, and label all slopes.

It is possible to couple the inductors in this manner, and cause one of the inductor current ripples to go to zero, in any converter in which the inductor voltage waveforms are proportional.

13.5 Over its usable operating range, a certain permanent magnet material has the B–H characteristics illustrated by the solid line in Fig. 13.55. The magnet has length $\ell_m = 0.5$ cm, and cross-sectional area 4 cm^2. $B_m = 1$ T. Derive an equivalent magnetic circuit model for the magnet, and label the numerical values of the elements.

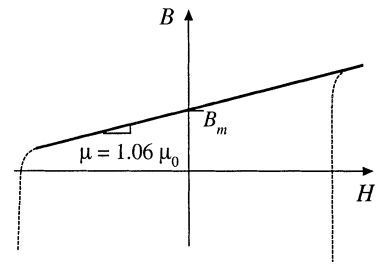

Fig. 13.55 B–H characteristic of the permanent magnet material for Problem 13.5.

13.6 The two-transistor forward converter of Fig. 6.27 operates with V_g = 300 V, V = 28 V, switching frequency f_s = 100 kHz, and turns ratio n = 0.25. The dc load power is 250 W. The transformer uses an EC41 ferrite core; relevant data for this core is listed in Appendix D. The core loss is given by Fig. 13.20. The primary winding consists of 44 turns of #21 AWG wire, and the secondary winding is composed of 11 turns of #15 AWG wire. Data regarding the American wire gauge is also listed in Appendix D.

(a) Estimate the core loss of this transformer

(b) Determine the copper loss of this transformer. You may neglect proximity losses.

13.7 The two-transistor forward converter of Fig. 6.27 operates in CCM with V_g = 300 V, V = 28 V, switching frequency f_s = 100 kHz, and turns ratio n = 0.25. The dc load power is 250 W. The transformer uses an EC41 ferrite core; relevant data for this core is listed in Appendix D. This core has window height ℓ_w = 2.78 cm. The primary winding consists of 44 turns of #24 AWG wire, and the secondary winding is composed of 11 turns of #14 AWG wire. Each winding comprises one layer. Data regarding the American wire gauge is also listed in Appendix D. The winding operates at room temperature.

(a) Determine the primary and secondary copper losses induced by the dc components of the winding currents.

(b) Determine the primary and secondary copper losses induced by the fundamental components of the winding currents.

(c) Determine the primary and secondary copper losses induced by the second harmonic components of the winding currents.

13.8 The winding currents of the transformer in a high-voltage inverter are essentially sinusoidal, with negligible harmonics and no dc components. The primary winding consists of one layer containing 10 turns of round copper wire. The secondary winding consists of 250 turns of round copper wire, arranged in ten layers. The operating frequency is f = 50 kHz, and the winding porosity is 0.8. Determine the primary and secondary wire diameters and wire gauges that minimize the total copper loss.

13.9 A certain three-winding transformer contains one primary and two secondaries. The operating frequency is 40 kHz. The primary winding contains a total of 60 turns of #26AWG, arranged in three layers. The secondary windings each consist of five turns of copper foil, one turn per layer. The foil thickness is 0.25 mm. The primary layers have porosity 0.8, while the secondary layer porosity is 1. The primary winding carries a sinusoidal current having rms value I, while each secondary carries rms current $6I$. The windings are not interleaved: the primary winding is closest to the center leg of the core, followed by secondary winding #1, followed by secondary winding #2.

(a) Sketch an MMF diagram illustrating the magnetic fields in the vicinity of each winding layer.

(b) Determine the increased copper loss, due to the proximity effect, in each layer.

(c) Determine the ratio of copper loss to dc copper loss, F_R, for the entire transformer windings.

(d) In this application, it is not feasible to interleave the primary winding with the other windings. However, changing the conductor size is permissible. Discuss how the windings could be better optimized.

13.10 A transformer winding contains a four-layer primary winding, and two two-layer secondary windings. Each layer of the primary winding carries total current I. Each layer of secondary winding #1 carries total current $1.5I$. Each layer of secondary winding #2 carries total current $0.5I$. All currents are sinusoidal. The effective relative conductor thickness is $\varphi = 2$. The windings are partially interleaved, in the following order: two primary layers, followed by both layers of secondary #1, followed by both layers of secondary #2, and finally the two remaining primary layers.

(a) Sketch an MMF diagram for this winding arrangement.

(b) Determine the increased copper loss, due to the proximity effect, for each layer.

(c) Determine the increase in total transformer copper loss, due to the proximity effect.

13.11 A single-output forward converter contains a transformer having a noninterleaved secondary winding with four layers. The converter operates at $D = 0.3$ in CCM, with a secondary winding current waveform similar to Fig. 13.38.

(a) Estimate the value of φ_1 that minimizes the secondary winding copper losses.

(b) Determine the resulting secondary copper loss, relative to $I_{rms}{}^2 R_{dc}$.

13.12 A schematic diagram and waveforms of the isolated SEPIC, operating in CCM, are given in Figs. 6.37 and 6.38.

(a) Do you expect the SEPIC transformer to contain an air gap? Why or why not?

(b) Sketch the SEPIC transformer *B–H* loop, for CCM operation.

(c) For CCM operation, do you expect core loss to be significant? Explain your reasoning.

(d) For CCM operation, do you expect winding proximity losses to be significant? Explain your reasoning.